catalysts

MDPI

Review

Quantum Dots and Gold Nanoparticles as Scaffolds for Enzymatic Enhancement: Recent Advances and the Influence of Nanoparticle Size

Gregory A. Ellis †, Scott N. Dean †, Scott A. Walper and Igor L. Medintz *

Center for Bio/Molecular Science and Engineering, Code 6900, U.S. Naval Research Laboratory, Washington, DC 20375, USA; gregory.ellis@nrl.navy.mil (G.A.E.); scott.dean.ctr@nrl.navy.mil (S.N.D.); scott.walper@nrl.navy.mil (S.A.W.)

* Correspondence: igor.medintz@nrl.navy.mil

† These authors contributed equally.

Received: 13 December 2019; Accepted: 31 December 2019; Published: 7 January 2020

Abstract: Nanoparticle scaffolds can impart multiple benefits onto immobilized enzymes including enhanced stability, activity, and recoverability. The magnitude of these benefits is modulated by features inherent to the scaffold–enzyme conjugate, amongst which the size of the nanoscaffold itself can be critically important. In this review, we highlight the benefits of enzyme immobilization on nanoparticles and the factors affecting these benefits using quantum dots and gold nanoparticles as representative materials due to their maturity. We then review recent literature on the use of these scaffolds for enzyme immobilization and as a means to dissect the underlying mechanisms. Detailed analysis of the literature suggests that there is a "sweet-spot" for scaffold size and the ratio of immobilized enzyme to scaffold, with smaller scaffolds and lower enzyme:scaffold ratios generally providing higher enzymatic activities. We anticipate that ongoing studies of enzyme immobilization onto nanoscale scaffolds will continue to sharpen our understanding of what gives rise to beneficial characteristics and allow for the next important step, namely, that of translation to large-scale processes that exploit these properties.

Keywords: enzyme; nanoparticle; biocatalysis; quantum dots; substrate channeling; scaffold

1. Introduction

Enzymatic catalysis is exquisite in its ability to enhance specific reaction rates by orders of magnitude using precisely selected substrates from within a milieu of other compounds [1]. This ability is highlighted in the thousands of "one-pot" reactions that are not only biocatalyzed simultaneously yet specifically in the metabolic network of a cell, but can occur in water at ambient pressure and temperature and can produce regio- and stereo-selective products [2–7]. It is no wonder that enzymes have been studied and engineered for a range of applications, including biodegradation/bioremediation of toxic compounds, chemical biosynthesis, and detection using biosensors, among others [2,6,8,9].

While solution-based enzymes have shown success in many applications, it can be desirable to immobilize them for a variety of reasons (highlighted below). This is evidenced by nature's use, and researchers' engineered exploitation, of metabolons (e.g., clustered TCA cycle enzymes) and scaffolds (e.g., cellulosomes of scaffoldin and cellulases) [3,10,11]. A range of both biotic and abiotic soluble scaffolds have been used to immobilize enzymes, including: cellular surfaces, peptides, proteins, DNA, polymers, metal-organic frameworks, and nanoparticles (NPs), among others [4,12–14]. NPs notably present unique features for enzyme immobilization, and two in particular—quantum dots (QDs) and gold-nanoparticles (AuNPs)—will be the subject of this review. Note that NPs are defined as a particle

between 1 and 100 nm in diameter [15,16]. The interested reader is directed to excellent reviews on other scaffolds for enzyme immobilization [4,12–14].

Herein, we first describe the benefits of enzyme immobilization and potential mechanisms underlying these advantages, followed by factors affecting these benefits—in particular, construct size. We then review progress on the use of QDs and AuNPs for enzyme immobilization within the last ~5 years with selected examples, and extend our apologies for any and all omissions. Our goal is to highlight the potential of nanostructuring enzymes onto QDs and AuNP for enhancing biocatalytic applications by reviewing the unique benefits that have already been elucidated and then extending this to an outlook for future work in both the near and long term.

1.1. Benefits of Enzyme Immobilization

Enzymes can be immobilized either as single copies or as multiple enzymes which are part of a multienzyme cascade [4,17–22]. Benefits of immobilizing single enzymes can include: (1) increased stability, (2) increased activity, (3) closeness and orientation to substrate, and (4) increased recoverability and reuse; whereas, the benefits of immobilizing multiple enzymes can include these plus: (5) increased (temporary) reaction rates, (6) bypassed intermediate toxicity, (7) bypassed off-target pathways/directed catalysis, (8) reaction order, and (9) modularity (Figure 1, Table 1) [4,10,23–30].

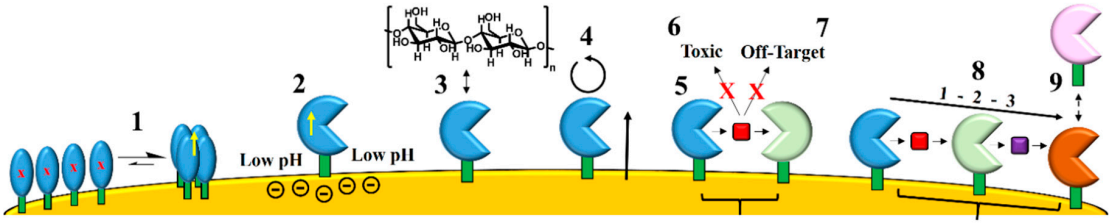

Figure 1. Enzyme immobilization can result in multiple benefits (1–9) [4,10,23–30].

Table 1. Potential Benefits of Enzyme Immobilization.

#	Benefit	Notes
1	Increased stability	Maintain quaternary structure due to subunit proximity; improved local environment
2	Increased activity	More favorable environment due to scaffold or surface chemistry, e.g., local pH closer to optimal enzyme pH
3	Closeness to substrate	Places enzyme in correct position and orientation relative to substrate
4	Increased recoverability and reuse	Easier isolation of enzyme-scaffold complex than free enzyme from reaction solution
5	Increased reaction rates	Substrate channeled between proximate enzymes can (temporarily, at least) increase overall pathway rates
6	Bypassed intermediate toxicity	Substrate channeled between proximate enzymes, minimizing any toxic activity of intermediates
7	Bypassed off-target pathways/directed catalysis	Substrate channeled between proximate enzymes, minimizing off-target reactions on intermediates
8	Reaction order	Dictating order of reaction by choosing which enzymes to place in proximity
9	Modularity	Modular tags allow interchangeability of enzymes to change cascade (and product) or make de novo cascades

In terms of benefits of immobilizing both single and multiple enzymes, enzyme immobilization can improve enzyme stability by keeping subunits in close proximity or affecting the local environment around the enzyme [17–21]. For example, the stability of an active tetrameric enzyme expressed as tagged, inactive monomers (tagged = enzyme with binding conjugation moiety epitope, e.g., His_6-tag) will depend upon the equilibration between the associated and dissociated states; conjugating those tags to a scaffold can enhance association by keeping the monomers in close proximity [19].

Conversely, immobilization can decrease the stability of some enzymes through unfavorable steric or Coulombic interactions [30,31]. Modeling, or empirical trials, can help determine the best location for conjugation tags and distance between enzymes and the scaffold [32–37]. Immobilization can also improve the catalytic activity of enzymes [4,19,38–44]. For example, charged scaffold surfaces can modulate the local pH environment near an enzyme closer to its optimum, without the need to change buffer pH that may affect other processes [21,24,45–48]. Similarly, scaffolds can create a "barrier to diffusion" and help retain substrates or intermediates near the surface (e.g., by Coulombic or hydrophilic/hydrophobic interactions), increasing the local concentration and improving enzymatic activity [24,45,46]. Immobilization can place enzymes in closer contact with substrates, facilitating activity [3,4,11]. A prime example is the cellulosome, where cellulases are attached to scaffoldin protein scaffolds on the cell surface; this places the cellulases in closer contact with the cellulose substrate and obviates the need for large cellulose polymers to enter the cell [3,11]. Finally, immobilization can improve recoverability and reuse of enzymes [2,7,18,49,50]. This would be particularly important for industrial processes if the enzyme is very expensive. Magnetic NPs are one example of a scaffold that has been investigated in this regard [2,7,18,49–52].

The immobilization of multiple enzymes in a biocatalytic cascade can add some additional benefits. By keeping the enzymes in close proximity, substrate channeling can potentially occur, where the passing of intermediate between two enzymes is enhanced versus bulk diffusion [4,10,26–28]. While the extent of the kinetic benefit of this effect may be short lived in some cases and is beyond the scope of this review—see [4,10,11,24–28,53,54] for more discussion on this topic—this effect can also help bypass toxicity of a harmful intermediate, bypass the pull of intermediate away in off-target pathways (whether reaction in another cascade or degradation), and help direct catalysis of an intermediate step (e.g., limiting isomerization). Further, in cases where multiple enzymes are immobilized site-specifically, reaction-order can be dictated to direct the pathway and/or increase activity. Finally, the use of orthogonal tags/docks between enzymes and scaffolds can allow for modularity and the design of de novo cascades linking enzymes together that do not associate in naturally occurring cascades [55–58].

Overall, enzyme immobilization can offer inherent benefits, and these can be particularly exploited when working at the nanoscale with NPs. Advantages of NPs include: (1) multiple mechanisms for enzyme attachment; (2) high surface area to volume ratios and corresponding high radii of curvature leading to relatively large distances between enzymes and limiting detrimental protein–protein interactions; (3) the potential for multi-point attachment of (multi-subunit) enzymes, allowing in some cases increased enzyme stability; (4) the ability to structure solvent up to ~2 × NP diameter, effecting many properties (e.g., pH gradients and boundary layers) that could affect substrate/intermediate/product partitioning; and (5) the ability to diffuse, whereas planar surfaces may have boundary layer and stagnation effects [19,22,42,59–64]. While many NPs have been used for enzyme immobilization (silica, magnetic, silver, etc.), herein we focus on recent examples using QDs and AuNPs. Both QDs and AuNPs are popular for immobilization due to certain shared characteristics, such as their crystalline nature which provides the potential for very uniform structure with low polydispersity. Since their spectral properties are closely regulated by their size, their spectra can even be used for quality control, in addition to their often-utilized properties as reporters or probes that can be used in various applications. While there are many potential benefits for immobilizing enzymes, numerous factors can affect the beneficial degree, or even liability, of immobilization. These factors are discussed in the following two subsections, and include: (1) immobilization chemistry, (2) scaffold material, (3) scaffold size, (4) scaffold:enzyme ratio, and (5) scaffold aggregation, among others [4,35].

1.2. Factors Affecting Immobilization Benefits—Immobilization Chemistry and Scaffold Material

In terms of immobilization chemistry, enzymes can be immobilized to a scaffold either covalently or non-covalently [4,32,34,37]. A common method of covalent non-specific conjugation is the use of homo-bifunctional organic linkers, such as those with one or both sides as an aldehyde (e.g., glutaraldehyde) or as an *N*-hydroxysuccinimide ester (NHS-ester) to bind amines (e.g., lysine epsilon

amine), or the use of hetero-bifunctional linkers where one side is amine reactive and the other is a thiol to bind to thiol-reactive scaffolds (e.g., AuNPs) [33,34]. For covalent site-specific conjugation, an enzyme cysteine (either natural or as a variant) can be bound to maleimide, with the other side of the linker bound to the scaffold [32]. Alternatively, in the case of citrate-stabilized AuNPs, an enzyme's cysteine can displace the weakly-bound citrate and covalently bind to the thiol-reactive AuNP [65–67]. For non-covalent attachment, common methods include charge/charge, hydrophobic, hydrogen bonding, and Van der Waals interactions between the enzyme and the scaffold [66]. In regards to QDs and AuNPs specifically, one advantageous method of non-covalent attachment is the use of a polyhistidine-tag (e.g., His_6) on one termini of the enzyme to coordinate Zn on the shell of core-shell CdSe/ZnS QDs or to coordinate to Ni^{2+}-nitrilotriacetic acid (Ni^{2+}-NTA) groups on the surface of AuNPs [4,68]. This method benefits from using an inherent purification method for many enzymes (His_6-tag) without requiring additional enzyme modification, as well as a relatively strong binding affinity (nM for His_6-QDs [69] to low μM for His_6-Ni^{2+}/NTA [68,70]). There are myriad other examples of covalent and non-covalent attachment strategies; the interested reader is directed to several excellent reviews [32,34,37]. Four important aspects of the conjugation chemistry emerge. First, the binding affinity of the attachment will dictate how often the enzyme is attached and presumably receiving the benefits of the scaffold. This is especially important when approaching concentrations close to the dissociation constant [68,69]. Second, site-specific attachment on enzymes can be less detrimental to activity, as one can avoid sites needed for activity such as active site residues [32]. Third, multiple attachment points can produce avidity affects onto the scaffold, improving association and/or improving enzyme stability; this may come at a cost of enzyme activity due to a reduction of allowed enzyme conformations [19,42,71]. Fourth, the distance of the linker (e.g., expanded bifunctional linkers with polyethylene-glycol, PEG, between reactive moieties), can positively (e.g., reduce steric hindrance) or negatively (e.g., minimize effect of local pH changes) affect immobilization benefits. While some of these aspects can be modeled *a priori*, sometimes a more empirical approach must be taken to determine the best immobilization chemistry [32,34,37].

In addition to immobilization chemistry, the scaffold material itself can affect the benefits of immobilization. As discussed above, many scaffolds, abiotic and biotic, are available [4]. The influence of scaffold material is illustrated by the effect of DNA on the coupled reaction of horseradish peroxidase (HRP) and glucose oxidase (GOx), which oxidizes glucose to D-glucono-δ-lactone and H_2O_2 then uses H_2O_2 to oxidize dyes such as 2,2′-azino-bis(3-ethylbenzothiazoline-6-sulfonic acid) (ABTS) [21,72–74]. When HRP and GOx were scaffolded onto negatively-charged DNA, the rate of the coupled reaction increased several fold, and this changed with distance between the enzymes. Initial indications were that this was due to a substrate channeling phenomenon. However, Idan and Hess illustrated that the effect was more likely due to a local change in pH, bringing the pH closer to the optimum for HRP [21]. Additional evidence for enzymatic enhancements due to scaffold-mediated environmental changes came from work by Zhao et al., who showed that HRP, GOx, malate dehydrogenase, and lactate dehydrogenase encased in DNA nanocages had increased activity [21,48]. Presumably, a positively-charged scaffold would not increase, and would perhaps decrease, the activity of these enzymes. Further, Klein et al. investigated a multienzyme cascade of amylase, maltase, and glucokinase on a DNA origami triangle in seven different enzyme confirmations, finding a 30-fold increase in pathway activity. The authors found that this was due to increased enzyme stability and a local environment affect (due to DNA surface affinity or a hydration layer) and not substrate channeling [47]. Another illustrative example is by Liu et al., who used a predominantly-lysine cationic bridge between two coupled enzymes (hexokinase and glucose-6-phosphate dehydrogenase) to facilitate substrate channeling of the dual-negatively charged intermediate [75]. A similarly-long neutral bridge did not show evidence of substrate channeling. Besides the charge effect, other scaffold materials bring inherent benefits. For example, iron-oxide (Fe_3O_4) NPs, or NPs containing Fe_3O_4, are magnetic, facilitating facile recoverability and reuse of conjugated enzymes [2,7,18,49–52]. Finally, NPs in particular can be manufactured with tight size tolerances in a range suitable for immobilization benefits (see below).

1.3. Factors Affecting Immobilization Benefits—Scaffold Size, Scaffold:Enzyme Ratio, and Scaffold Aggregation

In addition to the immobilization chemistry and scaffold material, three linked factors also affect immobilization benefits: scaffold size, scaffold:enzyme ratio, and scaffold aggregation. These factors are linked, as scaffold size will dictate surface area and, assuming a spherical scaffold such as NPs, surface curvature, and therefore the number of enzymes able to attach to the surface: smaller scaffolds will have higher relative surface area to volume ratios (SA:V) and surface curvature and therefore more room for a relatively larger number of enzymes to bind (Figure 2) [29–31,76–79]. Three recent papers have focused on the effects of scaffold size and scaffold:enzyme ratio; given their importance, we now highlight these results [29,31,76]. For the interested reader, we also note additional papers on the importance of scaffold size, see [30,77–79].

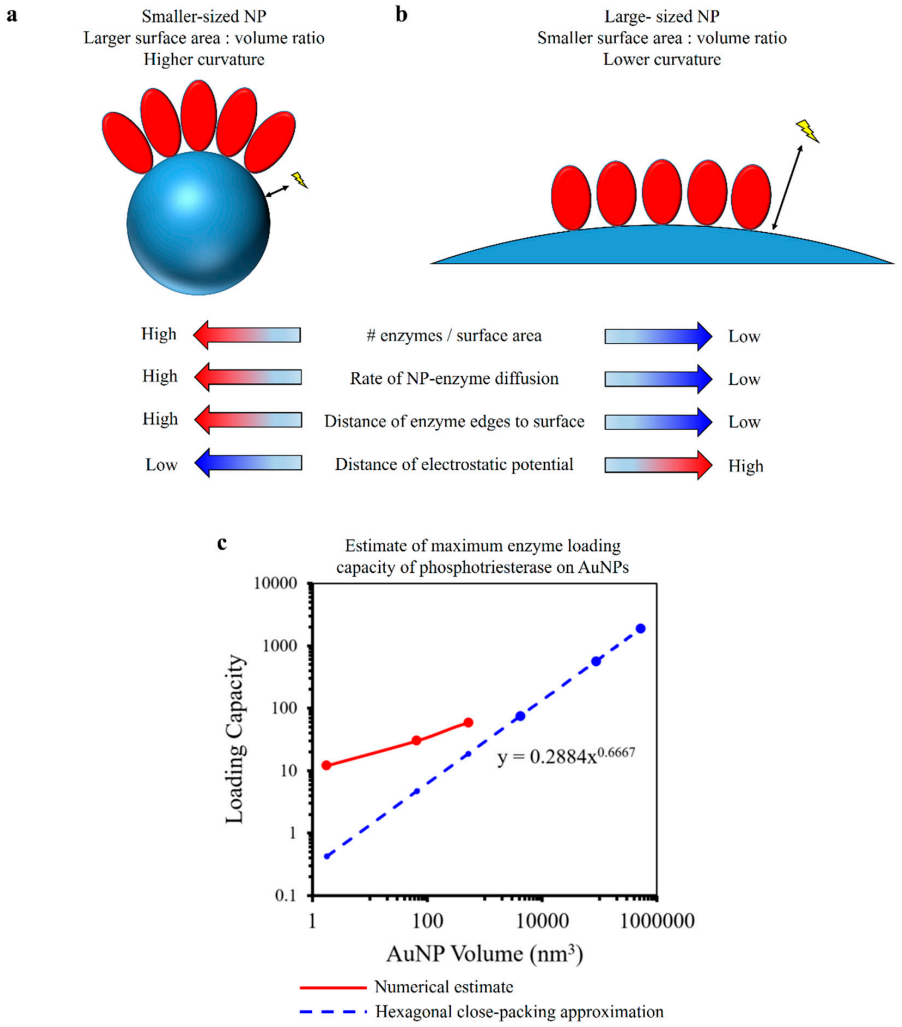

Figure 2. Nanoparticle (NP) size influences NP–enzyme complexes (**a**) A smaller-sized NP has a larger SA:V and higher curvature, resulting in a higher potential loading capacity of enzymes per SA, a higher rate of NP–enzyme diffusion (can limit overall activity less), a higher distance of enzyme edges to surface (can help stability), and a lower distance of electrostatic potential (less influence on local pH; indicated by arrows and lightning bolts) (**b**) A larger sized NP, conversely, has a smaller SA:V and a lower curvature. (**c**) Examining the AuNPs Breger et al. used in terms of AuNP volume, a numerical estimation and the hexagonal close-packing (HCP) approximation of the loading capacity indicate a relatively small gain in loading capacity for large increases in volume, which correlates to total Au used and presumably price. Initial values draw from Breger et al., and utilized for subsequent analysis here [76].

In the first paper, Lata et al. found that enzymes immobilized as a monolayer showed no trend of activity dependence on NP size (contrary to previous reports), but when immobilized as multilayers, showed a trend of decreasing activity with increasing NP size. Three enzymes from glycolysis were investigated immobilized on AuNPs of four different sizes: 5, 10, 20, and 50 nm [29]. The three enzymes were chosen to represent different enzyme classes: the isomerase glucose-6-phosphate isomerase (GPI), the oxidoreductase glyceraldehyde-3-phosphate dehydrogenase S (GAPDHS), and the transferase pyruvate kinase (PK). The conjugation chemistry used was to functionalize the AuNP with Ni^{2+}-NTA compounds and use these to bind His_6-tags on the enzymes. Importantly, the authors investigated the turnover number—k_{cat}, the Michaelis constant—K_M, and the enzyme efficiency—k_{cat}/K_M, for each condition and studied two situations: Where the enzymes were displayed as a monolayer on the AuNP, and where the enzymes were displayed as multilayers on the AuNP. For the formation of monolayers, the NTA-AuNPs were standardized to equal total surface area. Each of the enzymes decreased in activity when immobilized on the AuNP under the authors' conditions. For the monolayer, there were statistically significant modulations of k_{cat} with size but no trend; however, the authors note these should be taken with caution due to the experimental setup (Figure 3a). For the multilayer, there was a significant decreasing trend in k_{cat} with increasing AuNP size (Figure 3b); the authors speculate this may be due to an increased number of multilayers on the larger AuNPs limiting the number of active enzymes on the AuNP (e.g., by hindering access to substrate or sterically hindering needed enzyme conformational changes). The authors do not know why more multilayers form on larger AuNPs, but speculate it could be due to: (1) decreased curvature leading to decreased distance between enzymes, closer packing, and more enzyme–enzyme interactions; (2) the positively-charged His_6-tag interacting with the negatively-charged enzymes (would preserve orientation), since enzyme packing is likely due to weak protein–protein electrostatics; and (3) enzyme crowding, since at high concentrations enzymes tend to form complexes with each other (also helps stabilize them in a folded state). Altogether, the authors found that for all three enzyme classes, larger AuNPs had higher total activity per AuNP (since more enzymes were attached), and smaller AuNPs had higher activity per enzyme as multilayers.

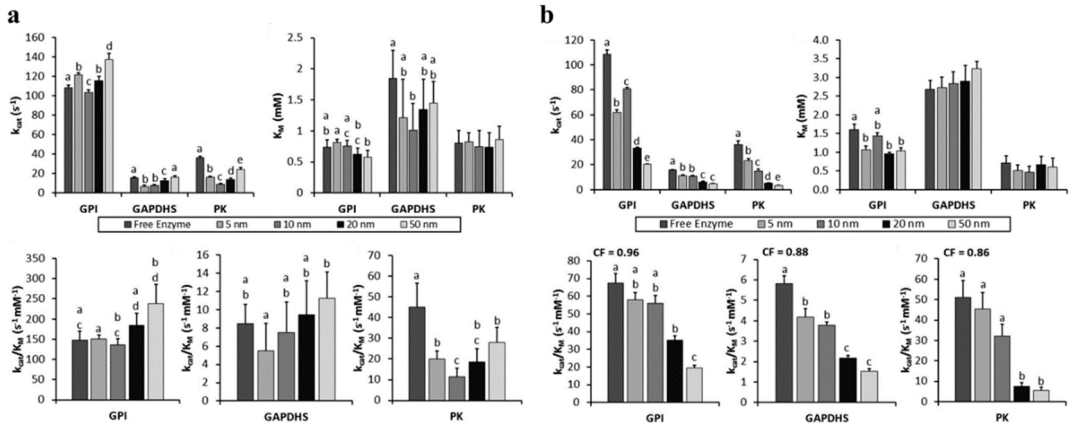

Figure 3. Kinetics of the tethered enzymes as a monolayer and in multilayers. Activity was measured for each enzyme on various sizes of AuNP with varying amounts of substrate. Values for k_{cat} and K_M were calculated using Michaelis–Menten kinetics. (**a**) Kinetics of enzymes in a monolayer. The turnover number (k_{cat}) displayed no significant trend, irrespective of enzyme type (top left). K_M also showed no significant difference for any enzyme as the size of AuNP changed (top right). Both kinetic variables were then utilized to plot enzyme efficiency (k_{cat}/K_M) yielding no clear trend for change in efficiency as AuNP size increased (bottom); (**b**) Kinetics of multilayer enzymes. The turnover number (k_{cat}) decreased as AuNP size increased, irrespective of enzyme type (top left). However, K_M showed no significant difference for any enzyme as the size of AuNP changed (top right). Both kinetic variables were then utilized to plot enzyme efficiency (k_{cat}/K_M) yielding a substantial decrease in efficiency as AuNP size increased with correlation factors as high as 0.96 for GPI. Pearson's correlation factors (CF) were calculated by using *Excel*. (**a**,**b**) Error bars show standard deviation. All comparisons among sizes

for a given enzyme were performed using a Student's *T* test with unequal variance (*Excel*, Microsoft Corporation, Redmond, VA, USA); dissimilar letters denote significance at $p < 0.05$, no letters indicate no significance. Reproduced with permission from ref. [29]. Copyright 2015 American Chemical Society, Washington, D.C., USA.

Interestingly, Lata et al. also include a table of other studies of AuNP sizes, see Table 2 below. The authors note that due to different methodologies, it is difficult to make general statements. Note, however, that there does seem to be a "sweet spot" for each, and that the activity (however measured) tends to go down if the NP is too large, which is a pretty consistent finding in most studies.

Table 2. Prior studies involving effects of NP size on bound enzyme activity.

Enzyme	Binding	NP	NP Size (nm)	k_{cat} (s^{-1})	K_M (μM)	k_{cat}/K_M (s^{-1} μM^{-1})	Specific Activity [3]	Relative Activity [4]	Ref
α-chymotrypsin	Amine	Polystyrene	110	20	31.7	0.63	NA	NA	[77]
-	-	-	270	18.6	40.9	0.46	NA	NA	
-	-	-	490	19.4	66.4	0.29	NA	NA	
-	-	-	1000	15.4	63.7	0.24	NA	NA	
Lipase [1]	Adsorption	Gold	13.1	18	9.5	1.89	NA	NA	[79]
-	-	-	25.2	18.3	14.1	1.3	NA	NA	
-	-	-	37.5	19.6	15.7	1.25	NA	NA	
-	-	-	50.8	19.1	17.1	1.12	NA	NA	
-	-	-	69.6	17.9	18.1	0.99	NA	NA	
Glucose oxidase	Amine	Fe_3O_4	5	NA	NA	NA	5800	NA	[78]
-	-	-	26	NA	NA	NA	5100	NA	
-	-	-	51	NA	NA	NA	3800	NA	
Lysozyme [2]	Adsorption	Silica	4	NA	NA	NA	NA	65	[30]
-	-	-	20	NA	NA	NA	NA	42	
-	-	-	100	NA	NA	NA	NA	38	

[1] *Candida rugosa* lipase. [2] Chicken egg lysozyme. [3] Specific Activity (U/g protein). [4] Relative Activity (%) at 100 nm^2 Surface Area. NA, Not acquired. Reproduced with permission from ref. [29]. Copyright 2015 American Chemical Society, Washington, DC, USA.

In the second paper, Tadepalli et al. investigated both NP size and curvature fairly independently and found that enzyme activity decreased with increasing NP size; the authors attributed this to a slower rate of diffusion rather than decreased curvature [31]. Tadepalli et al. focused on the enzyme HRP and adsorbed it onto AuNPs. First, they did this on differently sized AuNPs of diameters 10.1 nm (NP10), 20.8 nm (NP20), 30.5 nm (NP30), and 39.7 nm (NP40) determined by TEM (confirmed by DLS). HRP adsorbed (saturated) on NP10 and NP20 showed an increase in hydrodynamic diameter of ~4.5 nm, whereas HRP adsorbed on NP30 and NP40 showed an increase of only ~3 nm; the authors speculate that this is lower than the expected 8 nm increase due to HRP spreading during adsorption, and that the difference between AuNPs is due to HRP remaining in a more natural state on smaller AuNPs. The authors bolster this with circular dichroism (CD) spectroscopy and tryptophan fluorescence spectroscopy data showing more native secondary structure on NP10, and state this is likely due to the high curvature causing less protein changes during adsorption, consistent with previous publications [31] (and references within). For these constructs, with increasing size, the k_{cat} of HRP decreased (Figure 4a), the K_M increased then decreased (Figure 4b), and the k_{cat}/K_M decreased (Figure 4c). The authors attributed the decrease in k_{cat} to slower diffusion kinetics of HRP-NP. The increase of K_M for NP10 was attributed to potential crowding at the high curvature (with less free volume available, Table 3) reducing active site availability, whereas the decrease in K_M for the larger NPs was due to HRP unfolding easing crowding and allowing for more active site availability. To separate the effects of size and curvature, the authors shrewdly compared an 80 nm AuNP (NP 80) (Figure 4d) to a constructed gold superstructure (SS) of 10 nm AuNPs grown on a 60 nm AuNP (NP60 alone; SS60 as the superstructure). NP80 and SS60 had the same diameter but SS60 had significantly more curvature (Figure 4e). HRP adsorbed on these had a similar k_{cat} between SS60 and NP80 but lower than NP60; the authors speculate that the slightly better HRP native structure on the high curvature SS60 was overweighed by the required longer time of substrate trying to reach the

active site of HRP in the SS60 curved features, and that the main driver was a slower diffusion overall of the larger structures and not curvature (Figure 4f). Conversely, HRP K_M was considerably higher with SS60 than either NP60 or NP80; the authors speculate that this is due to limited availability of the active site due to the high curvature of SS60, and indicates curvature could be more important (at least in this case) than overall size for K_M (Figure 4g).

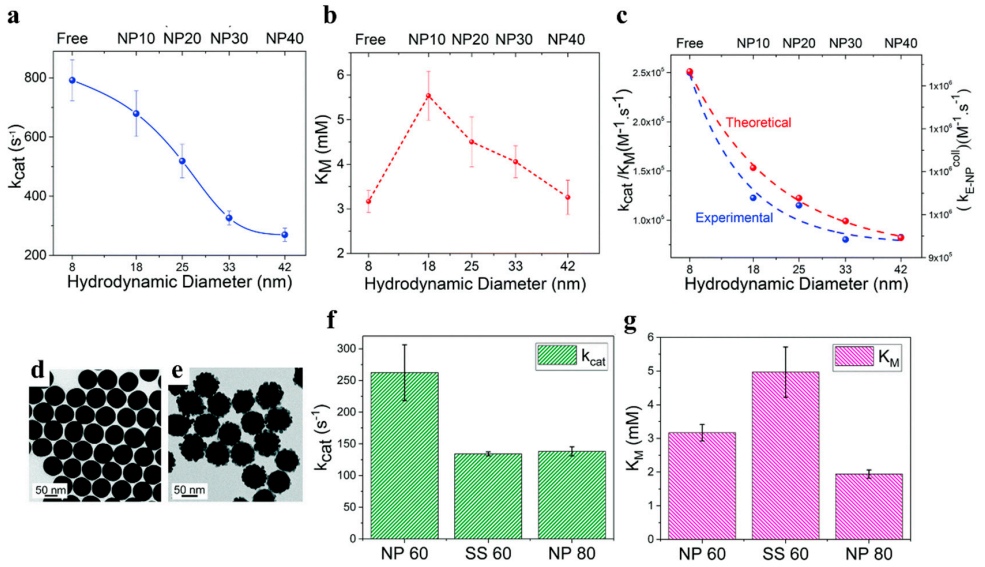

Figure 4. Kinetics of HRP on different sizes and configurations of AuNP (**a**) Turnover number (k_{cat}) of free HRP and NP + HRP conjugates; (**b**) Michaelis–Menton constant (K_M) as a function of the hydrodynamic diameter of the NP; (**c**) Plot showing the catalytic efficiency (k_{cat}/K_M) of free and size-controlled bionanoconjugates in comparison to a theoretical model (not accounting for secondary structure loss); (**d**) Representative TEM image of 80 nm AuNPs (NP 80); (**e**) Bright field TEM image of 60 nm AuSS (SS60); (**f**) Plot showing the k_{cat} values of 60 nm NP (NP 60), 60 nm SS, and 80 nm NP; (**g**) Plot showing the K_M values of 60 nm NP, 60 nm SS, and 80 nm NP. Reproduced with permission from ref. [31]. Copyright 2017 The Royal Society of Chemistry, London, United Kingdom.

Table 3. Estimation of the number of horseradish peroxidase (HRP) per NP.

AuNP Diameter (nm)	AuNP Surface Area (nm^2)	AuNP Volume (nm^3)	# HRP/AuNP	# HRP/AuNP SA nm^2	Estimated HRP Volume (nm^3) [1]	Approx. Volume Occupied by HRP per nm^2 SA (nm^3) [2]	# NRP/AuNP Volume nm^3
10	314.16	523.60	46	0.15	3 × 4.5 × 5 (67.2)	9.78	0.088
20	1256.64	4188.79	236	0.18	3 × 4 × 3.5 (42)	7.88	0.056
30	2827.43	14,137.17	571	0.2	3 × 3.5 × 2.5 (26.25)	5.29	0.040
40	5026.55	33,510.32	1414	0.28	3 × 3 × 2 (18)	5.06	0.042

[1] Parenthesis indicate total estimated volume multiplied out. HRP is 3 × 6.5 × 7.5 nm^3 before immobilization [80]. HRP secondary structure decreases when immobilized; volumes estimated based on diameter reduction with increased AuNP size. [2] Volume occupied by HRP decreases with particle size based on assumptions above. This indicates that less free volume is available with decreased AuNP size due to HRP crowding [31]. AuNP volume and last column derived from ref. [31]. Adapted with permission from ref. [31]. Copyright 2017 The Royal Society of Chemistry, London, United Kingdom.

In the third paper, Breger et al. recently examined enzyme activity with differently sized NPs under two conditions—fixed enzyme density and fixed enzyme diameter—and again found that there was a "sweet- spot" of low NP size and low enzyme coverage that produced the highest activity [76]. Breger et al. examined the activity of the enzyme phosphotriesterase (PTE) on differently sized AuNPs. Phosphotriesterase catalyzes the hydrolysis of phosphotriester bonds; its activity can be monitored by the hydrolysis of the pesticide metabolite and chemical warfare simulant paraoxon into *p*-nitrophenol (absorbance at 405 nm) and diethyl hydrogen phosphate. Critically, the authors examined the effect of

AuNP size in two regimes: Fixed enzyme density, and fixed NP diameter (Figure 5a). The authors concluded that there was a "sweet-spot" of a small diameter AuNP with fairly low enzyme coverage (Figure 5b, Tables 4 and 5) [76]. Note that this is relative to the efficiency of each PTE. The authors note that this is consistent with other reports where the most enhancement was seen with low enzyme:NP ratios [19,22,39,81,82]. Why is there a "sweet-spot" at all in regards to NP size? The authors speculate that this could be due to a relief of ligand crowding (nitrilotriacetic acid modified thioctic acid, TA-NTA) with an increase in curvature (decrease in size) as a result of released steric hindrance, and/or it could be due to an increase in product solubility/diffusivity in the AuNP hydration layer. The hydration layer could also help with product partitioning/product release; in fact, product release from enzymes is a frequent rate-limiting step [83]. It is noteworthy that colloidal NPs can restructure solvent to ~2× their diameter [64], which can affect pH, ion gradients, density, charge effects, boundary layers, etc. [62]. Another benefit to high-curvature NPs as scaffolds is their dynamic/diffusive nature vs. enzymes on a planar surface which will be affected by a boundary layer and possible stagnation effects [22]. Regardless, the effect of smaller NPs trending to larger enhancements have been seen in many systems [22,38,39,41–44,81,82]. Also note that the AuNP is also likely stabilizing PTE in an active confirmation, as discussed by the authors.

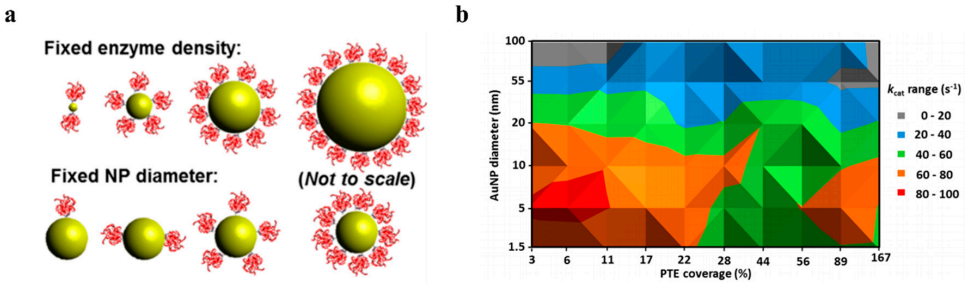

Figure 5. Kinetics of enzymes immobilized at fixed enzyme density or fixed NP diameter. (**a**) Schematic highlight the two different experimental formats utilized in Breger et al. A fixed enzyme density keeps the coverage per unit area of the NP constant across the NP size series while the fixed NP diameter varies the number of enzymes per NP while keeping the NP size constant. Note that both formats kept the enzyme concentration constant; (**b**) Plot of binned k_{cat} value ranges as a function of AuNP diameter and %PTE coverage in a topographical format. Note values for the 100 nm AuNPs at lowest coverage were not collected and are extrapolated here. Reproduced with permission from ref. [76]. Copyright 2019 American Chemical Society, Washington, D.C., USA.

Table 4. Averaged enzyme activities for fixed NP diameter format on 10 nm AuNPs.

PTE:AuNP	% NP Surface Coverage	k_{cat} (s^{-1})	K_M (μM)	k_{cat}/K_M (mM^{-1} s^{-1})	% Increase k_{cat}	(Extra) PTE per AuNP	(Extra) PTE/(Extra) AuNP
1	3	61.9	282	260	476	3.8	0.06
2	6	76.1	318	274	585	9.7	0.66
4	11	79.2	304	299	609	20.4	1.72
8	22	67.2	328	254	517	33.4	1.69
16	44	55	297	185	423	51.7	−1.76
32	89	58.4	286	220	449	111.8	NA
~PTE	-	13	72	181	-	-	-

Columns from Breger et al.: "PTE:AuNP" is the approximate ratio of PTE to AuNP; "% NP surface coverage" is calculated by the number of PTEs and the AuNP surface area; and "k_{cat}", "K_M", and "k_{cat}/K_M" is determined experimentally. Additional columns calculated based on these data (see Appendix A, Table A1 for calculations): "% increase k_{cat}" is k_{cat} relative to free PTE. "(Extra) PTE per AuNP" is the number of relative PTEs gained from each AuNP particle due to the increase in conjugated activity. If AuNP costs less than this factor over the cost of PTE, it is more economical to immobilize. "(Extra) PTE/(Extra) AuNP" is the number of additional conjugated PTEs divided by the number of additional AuNPs needed to achieve the same number of turnovers as 32:1 PTE:AuNP. If AuNP costs less than this factor over PTE, then that coverage is better than the highest coverage reported here (32:1 PTE:AuNP). Error ranges removed for clarity but are in referenced publication. Initial values draw from Breger et al. and utilized for subsequent analysis here [76].

Table 5. Averaged enzyme activities for fixed enzyme density format for low coverage conditions.

AuNP Diameter (nm)	PTE:AuNP	k_{cat} (s^{-1})	K_M (μM)	k_{cat}/K_M (mM^{-1} s^{-1})	% Increase k_{cat}	(Extra) PTE per AuNP	(Extra) PTE/(Extra) AuNP
1.5	1.25	59.1	222	265	721	7.8	0.75
5	1.5	71.3	583	122	870	11.5	1.41
10	6	81.2	443	187	990	53.4	7.37
20	24	59.0	328	186	720	148.7	15.35
55	182	54.3	655	82	662	1023.2	154.81
100	601	36.9	198	190	450	2103.5	NA
~PTE	-	8.2	6.7	130	-	-	-

Columns from Breger et al.: "AuNP diameter (nm)" is the diameter AuNP used for conjugation. "PTE:AuNP" is the approximate ratio of PTE to AuNP; "% NP surface coverage" is calculated by the number of PTEs and the AuNP surface area; and "k_{cat}", "K_M", and "k_{cat}/K_M" is determined experimentally. Additional columns calculated based on these data (see Appendix A, Table A2, for calculations): "% increase k_{cat}" is k_{cat} relative to free PTE. "(Extra) PTE per AuNP" is the number of relative PTEs gained from each AuNP particle due to the increase in conjugated activity. If AuNP costs less than this factor over the cost of PTE, it is more economical to immobilize. "(Extra) PTE/(Extra) AuNP" is the number of additional conjugated PTEs divided by the number of additional AuNPs needed to achieve the same number of turnovers as 32:1 PTE:AuNP. If AuNP costs less than this factor over PTE, then that coverage is better than the highest coverage reported here (32:1 PTE:AuNP). Error ranges removed for clarity but are in referenced publication. Initial values draw from Breger et al., and utilized for subsequent analysis here [76].

In order to more methodically delve into the impact of differently sized NPs on enzyme activity, we performed a literature search of articles that have reported the effects of QDs and AuNPs of different sizes on displayed enzyme activity that include reported k_{cat} values, extracting kinetic parameters and NP characteristics from tables and text. This totaled to 78 observations from 9 independent studies. Their effects on k_{cat} relative to free enzyme, the NP diameter, and ratio of the NP to the enzyme were then compiled. Other parameters, including NP composition, functionalization, enzyme used in the study, V_{max}, K_M, k_{cat}/K_M, and associated errors were also included, if available. The data are provided in Table S1 (Supplementary Materials).

Following normalization to the reported free enzyme k_{cat} (dividing reported k_{cat} enzyme-NP complexes by the k_{cat} for the free enzyme in the above mentioned dataset), the fold-changes were plotted, and a simple linear regression was performed. The results of this compilation are shown in Figure 6. For QDs, the relationship between fold-change in k_{cat} as a function of diameter is negative, with a slope of −0.30 (Figure 6a). Although there are fewer studies available to provide AuNPs-enzyme data for this analysis, there may be, like the QD-enzyme data, an apparent negative correlation between increasing AuNP size and the change in k_{cat} relative to free enzyme, where the correlation between fold-change in k_{cat} and diameter was −0.37 (Figure 6b). Since AuNPs can have a large range of possible diameters and have been tested with enzymes out to >100 nm, we truncated the *x*-axis to include ≤50 nm.

Since very few studies reporting differing enzyme:AuNP ratios are available and would largely represent data from a single source (Breger et al.), analysis for difference in k_{cat} as a function of NP ratio was only performed for QDs. Data were further categorized into small (<5 nm) or large (≥5 nm) diameters, to determine trends. From this, we can see that QDs likely have an optimal diameter range and enzyme:QD ratio, where for smaller QDs (<5 nm) the enzyme:QD ratios are noticeably more impactful on k_{cat} than for their larger counterparts; for both, lower enzyme:QD ratios appear more favorable for increasing k_{cat}. Concretely, the correlation between fold-change in k_{cat} and diameter was −0.30 while the correlation between fold-change in k_{cat} and enzyme:QD ratio was −0.4. Importantly, the negative relationship between fold-change in k_{cat} and enzyme:QD ratio is stronger for the small diameter QDs (−0.47), while the relationship between fold-change in k_{cat} and enzyme: QD ratio for large diameter QDs is weaker (−0.30) (Figure 6c).

Although the correlations are relatively weak as a result of relatively few studies reporting kinetic parameter values (i.e., k_{cat}, V_{max}, K_M) and, thus, the difference in correlation coefficients are not significant ($p = 0.2$; Fisher *z*-transformation), overall the trends observed here are consistent with the hypotheses put forward by several reports, suggesting an apparent positive relationship between larger enhancements and the use of smaller NPs, which has been demonstrated in many systems as stated in

the previous section [22,38,39,41–44,81,82]. In addition, the noticeable difference between small (<5 nm) or large (≥5 nm) diameter QDs at different enzyme: QD ratios, with most enhancement in k_{cat} seen in both small-diameter QDs and low enzyme: QD ratio, supports the "sweet-spot" results of Breger et al., discussed above [76]. In addition, the accumulation of more work reporting the impact of NP attributes on kinetic parameters of immobilized enzymes will significantly improve the confidence in observed trends and may allow for greater use of modeling of optimal NP characteristics in the future.

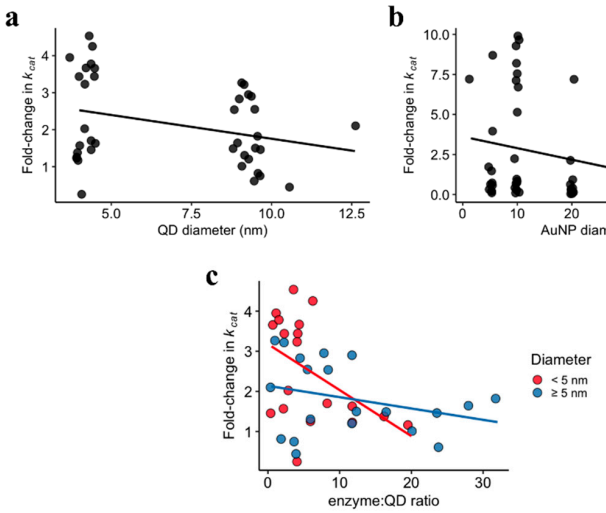

Figure 6. The relationship between fold-change in k_{cat} as a function of quantum dot (QD) and AuNP diameter and enzyme:NP ratio. (**a**) Linear fit of QD diameter and fold-change in k_{cat}. (**b**) Linear fit of AuNP diameter and fold-change in k_{cat}. (**c**) Shows the fold-change in k_{cat} as a function of enzyme: QD ratio colored by small (<5 nm) or large (≥5 nm) diameters.

Finally, the above examples illustrate scaffolds at the nanoscale (≤100 nm), which can have some unique qualities. Interestingly, going to larger sizes (microscale, >100 nm) can decrease the benefits from these types of scaffolds. One example is from the work of Mukai et al. [84]. In this work, the authors used 500 nm Ni^{2+}-NTA functionalized silica particles attached to the 10 enzymes of glycolysis (the 10 enzymes were split between three particles). When compared to free enzymes, the immobilized enzymes were overall less active, consuming less glucose and producing less lactate; however, the amount of lactate produced per glucose used was enhanced. It is not known, but could be anticipated, that using smaller NPs could have enhanced the overall production of lactate over free enzymes.

In addition to the size of the scaffold itself, scaffolds can aggregate into "clusters" (see also below). This clustering can be particularly advantageous for multienzyme cascades; reaction rates can increase significantly as intermediates are more likely to encounter another enzyme versus escape into bulk solution. This was illustrated by Castellana et al. [85]. The authors calculated that for a multienzyme cascade with an unstable intermediate, under their set of enzymes and conditions, the optimal size of aggregates was ~260 nm and distance between aggregates was 6.5 µm. They further estimated that flux would increase 6-fold for a 2-step cascade to over 100-fold for a 3-step cascade vs. free cellular enzymes.

2. Enzyme Immobilization on QDs

QDs are luminescent semiconductor nanoscale crystals that have begun to be widely employed in both fundamental research and technical applications as a result of their unique optical and electronic properties, including size-dependent photoluminescence caused by the absorption of light generating excitons followed by electron–hole recombination. Colloidal QDs, which have a high surface area to volume ratio, can be synthesized from a range of semiconductor materials, but among the most common are CdSe, CdTe, and core/shell CdSe/ZnS and CdTe/ZnS. For the core/shell QDs, the core (e.g., CdSe) is

surrounded by a shell (e.g., ZnS) that helps protect the core from oxidation and leaching, and improves the overall photoluminescence yield; thicker ZnS shells (e.g., 4–6 monolayers) give more protection whereas thinner ZnS shells (1–2 monolayers) produce higher photoluminescence. Hydrophilic ligands are then appended onto QDs to endow water solubility as well as additional stability and protection. In terms of their desirable photoluminescence properties, QDs can have a high quantum yield, high molar extinction coefficients, broad absorption windows, narrow photoluminescence windows over an overall broad range, large effective Stokes shifts, stability, resistance to photobleaching, and size-tunable photoluminescence, among other interesting properties [86–88]. Several common applications utilizing QDs have emerged including theranostics, cellular imaging, in vitro and in vivo biosensing, and photodetection. Among the biological applications of QDs, one of the most promising is their bioconjugation to enzymes where their increase in study has been in part due to their recently-established relationship in the enhancement in activity for various enzymes, including beta-galactosidase [40,89], alkaline phosphatase [41], trypsin [90], phosphotriesterase [39], and others.

In recent years, research groups have examined the effects that QDs have on enzymatic activity by immobilizing different enzymes on QDs—commonly CdSe/ZnS (core/shell)—with diameters generally smaller than other NP counterparts: ~3 nm to ~15 nm. The determination of diameters of QDs and NPs more generally is measured by transmission electron microscopy (TEM) and dynamic light scattering (DLS), where they are typically found to be uniform and devoid of large polydispersity due to their crystalline nature. In addition, since their spectral properties are tightly bound to their size, these properties can further enable quality control of the QDs used in experiments and in their various applications.

The most popular bioconjugation technique for immobilization involves the metal-affinity coordination of the QD with a polyhistidine tag engineered onto the enzyme, whose popularity may in part be due to the very common usage of polyhistidine tags in protein expression. This strategy also conveniently enables control over both the number and placement of enzymes on the QD surface in a site-specific manner allowing oriented enzyme immobilization, and although the enzyme movement has some degrees of freedom of movement around this site, this facilitates a largely tunable and controlled bioconjugation process [35,91,92].

In order to increase the biocompatibility of the QD surface to enzymes, the QD surface is generally functionalized with a surface ligand, the most popular of which is where the QDs are solubilized with a dihydrolipoic acid-zwitterionic compact ligand (CL4) [93,94]. Although other coatings have been investigated in the context of QD-enzyme activity enhancement, including amine, acetyl, methoxy, hydroxy, carboxy, and polyethylene glycol-CL4 [90], certain QD coatings such as CL4 demonstrate better solubility, high biocompatibility, maintain high quantum yields, and long-term stability across a broad pH range, each of which may be a relevant feature for consideration when investigating QD-associated impacts on enzymatic activity.

Accumulating work has demonstrated the enhancement of enzyme activity for both single-enzyme and multi-enzyme systems for cascade reactions following immobilization to QDs. In regards to single enzyme systems, recent work with phosphotriesterase (PTE) assembled to CdSe/ZnS core/shell QDs, which emitted at either 525 nm (4.3 ± 0.5 nm diameter) or 625 nm (9.2 ± 0.8 nm diameter) demonstrated that both QDs significantly enhanced immobilized enzymatic activity compared to enzyme in free solution; the k_{cat} increased ~4-fold while the enzymatic efficiency (k_{cat}/K_M) increased ~2-fold [82]. Although the focus of this review is exclusively on the enhancement of enzymatic activity with enzymes immobilized to QDs, we note that several reports have also indicated striking improvements in enzymatic activity when the substrate is attached to QDs, particularly as proteolytic reporters [87,88,90,95–107].

In another detailed study on QD-associated enhancement of a single enzyme, Claussen et al. investigated the enhanced performance of the enzyme alkaline phosphatase (AP) immobilized on CdSe/ZnS core/shell QDs. They found that both the V_{max} and k_{cat} were improved with successful orientational control of AP placement relative to AP in free solution. Although the increase in these

performance metrics varied in magnitude from ~5% to ~25%, both 525 nm and 625 nm QDs showed improvements at all QD:enzyme ratios examined. Interestingly, the enhancement on the smaller 525 nm QDs (4.2 ± 0.5 nm) ranged from 14% to 23%, while the larger 625 nm QDs (9.2 ± 0.8 nm) only saw improvements measuring slightly less than 10% [41]. This study postulates that the higher surface curvature of the smaller QDs better promotes native enzyme configuration and lower enzyme-to-enzyme neighbor interactions than the larger QDs. The greatest enhancement in enzyme performance was noted when fewer enzymes were immobilized on the QDs and therefore further corroborates the aforementioned postulate. This report supports the idea that nanomaterial morphology, size, and orientation can significantly affect and improve enzymatic activity [42].

Further in-depth studies have been recently carried out by Das et al., where size-dependent CdSe QD-lysozyme interactions has been studied to establish the effect of adsorption-directed alterations to lysozyme secondary structure and the resulting impact to enzymatic activity, using a range of techniques including static and synchronous fluorescence spectroscopy to quantify QD–lysozyme binding isotherms, and circular dichroism. Lysozyme was assembled on 2.5 and 6.3 nm diameter CdSe QDs and investigated for resulting conformational changes depending on QD size and whether the QDs impacted lysozyme activity (Figure 7a). Their results showed that conformational changes in lysozyme occurred for both QDs and that the smaller, higher curvature 2.5 nm QDs were found to promote more protein α-helical structure (*via* circular dichroism) and greater enzymatic activity—here, lysis of Gram-positive bacterium *Micrococcus lysodeikticus*—compared to larger QDs [108] (Figure 7b). Specifically, increasing the 2.5 nm QD concentration from 20 nM to 50 nM decreased the percent helix content of lysozyme from 32.89% to 24.09%. Interestingly, the researchers observed that despite the relatively poor binding of lysozyme by the smaller 2.5 nm QDs, they produced greater enhancement of enzymatic activity compared with the larger 6.3 nm QDs, which in turn exhibited stronger binding but which probably resulted in more protein denaturation across the larger NP surface. This observation is supported by previous work by Vertegel et al., showing that the activity of lysozyme on silica NPs is size-dependent, where there was a clear correlation between surface curvature of NPs and protein α-helix structure, and resulting enzymatic activity [30]. Finally, in another publication in regards to QD:enzyme ratios, Tsai et al. showed that cellulase activity was enhanced only under certain parameters, namely smaller QDs were used at specific ratios, such as 1:5 (QD:enzyme) [109].

In regards to multistep enzymatic cascades, Vranish et al. recently demonstrated the value of QDs for pathway enhancement. The authors used a model glycolysis-derived dual enzyme system composed of pyruvate kinase (PykA) and lactate dehydrogenase (LDH), where the first enzyme catalyzes the reaction of adenosine diphosphate (ADP) and phosphoenol pyruvate (PEP) to pyruvate and adenosine triphosphate (ATP) and the second enzyme converts the pyruvate intermediate plus nicotinamide adenine dinucleotide (NADH) to lactate and NAD+. This coupled glycolysis system was co-localized to the surface of QDs emitting at either 525 (4.3 ± 0.6 nm diameter) or 605 nm (10.1 ± 0.1 nm × 4.5 ± 0.4, length × width) (Figure 8). Assembled to either of the QDs, the group showed that attachment of tetrameric LDH to both the spherical 525 nm QDs and rod-like 605 QDs yielded a significant activity enhancement in turnover of as much as 50-fold. Critically, when this complex was paired with PykA on the QD surface, their coupled activity as measured by k_{cat} was enhanced, by over 100-fold greater than their free enzyme counterparts. The scale of this enhancement is significant compared to previously reported figures which were normally between ~2- and 5-fold (see Table 6), possibly in part due to an increase in tetramer stability, in addition to other factors. Of note was the importance of the ratio of QD to enzyme, and the relative ratio of the PykA and LDH enzymes to one another. The best-observed specific ratio was found to be 8:4:1 (LDH/PykA/QD), as determined by NADH consumption. In their study, both the experimental data and kinetic simulations strongly indicated that the enhancement was the result of substrate channeling between the enzymes [19] (Figure 8b). Interestingly, unlike several other studies reporting the enhanced enzymatic activity at the interface of smaller rather than large NPs, Vranish et al. found the greatest increase in k_{cat} when the coupled PykA−LDH enzyme system colocalized on a QD surface of the larger, oblong 605 QDs with

length × width of 10.1 ± 1.0 nm × 4.5 ± 0.4 nm rather than the spherical 525 QDs of diameter 4.3 ± 0.6 nm. However, they did observe that the lowest ratios of enzymes on QDs displayed the highest activities for the coupled system, a trend consistent with that seen by Breger et al., with the AuNP-PTE system [76].

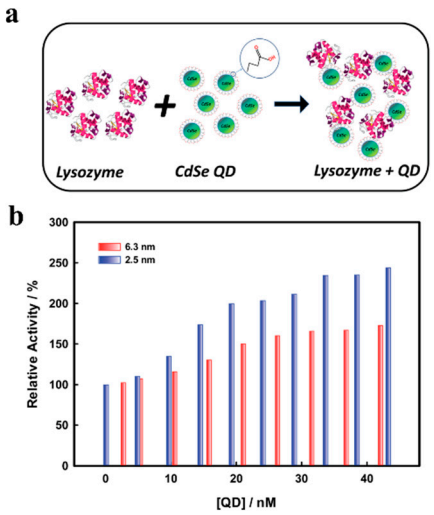

Figure 7. Effect of QD size on enzymatic enhancement of lysozyme. (**a**) Schematic of absorption of lysozyme on CdSe QDs. (**b**) Effect of concentration of QDs (2.5 to 52.5 nM) of sizes 2.5 nm and 6.3 nm on the enzymatic activity of lysozyme (5 μM). Reproduced (Adapted) from Ref. [108] with permission from The Royal Society of Chemistry, London, United Kingdom.

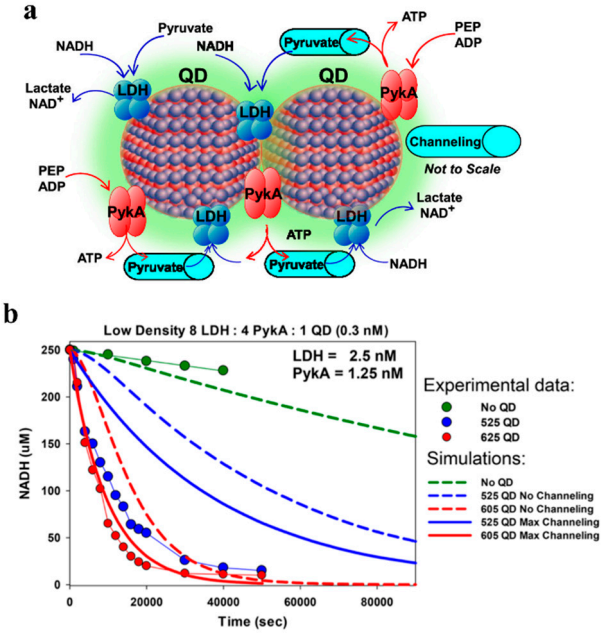

Figure 8. Enhancement of enzymatic activity with QDs. (**a**) Schematic of the coupled PykA−LDH enzyme system colocalized on a QD surface. The propensity of the enzymes to form cross-linked QD dimers and, to a lesser extent, trimers via the enzymes tetrameric polyhistidine tags is also schematically indicated. Note, not to scale. (**b**) Comparison of experimental data following sample NADH consumption with predictions of a kinetic model of the PykA/LDH cascade. The experimental data are denoted as points connected by thin lines of the same color, and the simulation results are given by thicker solid or dashed lines. The model and its kinetic parameters are discussed in the text including the approach used to simulate "Max channeling". Reprinted (adapted) with permission from [19]. Copyright 2018 American Chemical Society, Washington, D.C., USA.

Table 6. Overview of representative QD-immobilized enzymes.

Nanoparticles/Nanomaterials	Year	Surface Functionalization	Enzyme Attachment	Enzyme	Multimeric State of the Enzyme	QD Diameter (nm)	Enhancement (Compared to Free Enzyme)	Ref.
QDs (625 nm red emitting CdSe/ZnS core/shell)	2015	DHLA-CL4	His_6-tag	Beta-galactosidase	Tetramer	9.2 ± 0.8	3- to 4-fold enhancement in k_{cat};	[40]
QDs (525 nm green emitting CdSe)	2016	mercaptopropionic acid	His_6-tag	Lysozyme	Monomer	2.5	2- to 2.5-fold increase in lytic activity	[108]
QDs (655 nm red emitting CdSe/ZnS core/shell)	2017	CL4	His_6-tag	Horseradish peroxidase	Monomer	12.6 ± 0.9 × 6.7 ± 0.5 [1]	2-fold increase in k_{cat}	[44]
QDs (625 nm red emitting CdSe/ZnS core/shell)	2015	DHLA-CL4	His_6-tag	Alkaline phosphatase	Dimer	9.2 ± 0.8	25% increase in k_{cat}	[41]
QDs (625 nm red emitting CdSe/ZnS core/shell)	2015	DHLA-CL4	His_6-tag	PTE	Trimer	9.2 ± 0.9	2-fold increase in k_{cat} and k_{cat}/K_M	[82]
QDs (625 nm red emitting CdSe/ZnS core/shell)	2015	DHLA-CL4	His_6-tag	PTE	Dimer	9.2 ± 0.8	4-fold increase in initial rate; 2-fold increase in k_{cat}/K_M	[39]
QDs (525 nm green emitting CdSe/ZnS core/shell)	2017	CL4	His_6-tag	Beta-galactosidase	Tetramer	4.2 ± 0.5	3-fold increase in k_{cat}	[89]
QDs (605 nm emitting CdSe/ZnS core/shell)	2018	DHLA-CL4	His_6-tag	LDH and PykA	Tetramer	10.1 ± 1.0 × 4.5 ± 0.4	>50-fold increase in k_{cat} for couple enzymes	[19]
QDs (525 nm emitting CdSe/ZnS core/shell)	2014	GSH	His_6-tag	MenFDH	Monomer (three enzymes)	3.5	~4-fold increase in product formation	[110]
QDs (605 nm emitting CdSe/ZnS core/shell)	2013	DHLA	His_6-tag	CelAE	Monomer (two enzymes)	10	~2-fold increase in product formation	[109]

[1] 655 nm QDs were reported to be oblong and reported with separate length and width dimensions. Abbreviations: phosphotriesterase (PTE), lactate dehydrogenase (LDH), pyruvate kinase (PykA).

Another example of an in vitro cascaded reaction with QD-associated enhancement involved three enzymes found in the menaquinone biosynthetic pathway. In this study, Kang et al. reported the effect that localization of the three enzymes—MenF, MenD, and MenH—of the menaquinone biosynthetic pathway on CdSe/ZnS core/shell QDs with a diameter of ~3.5 nm had on activity. In the menaquinone biosynthetic pathway, MenF isomerizes chorismate to isochorismate, MenD (with thiamine diphosphate coenzyme) catalyzes a conjugate addition of α-ketoglutarate to isochorismate to produce 2-succinyl-5-enolpyruvyl-6-hydroxy-3-cyclohexadiene-1-carboxylate (SEPHCHC), and MenH SEPHCHC then undergoes pyruvate elimination catalyzed by MenH to give 2-succinyl-6-hydroxy-2,4-cyclo-hexadiene-1-carboxylate (SHCHC). SHCHC can lead to menaquinone through several additional steps. They demonstrated that the efficiency of the cascade reaction was dependent on the both the total number of enzymes per particle and the relative ratio of the three enzymes per particle, similar to the results seen in the dual enzyme system reported by Vranish et al. [19]. The reaction was observed to be more efficient when each particle contained a mixture of the three enzymes than when each particle contained only one type of enzyme and was most active when MenF was in excess over the other two enzymes—in a ratio of 20:5:5:2 (MenF/MenD/MenH/QD)—as determined by production of SHCHC from chorismate substrate (Figure 9). An interesting point was that complexation with QDs did not affect the catalytic activity of MenF, MenD, or MenH alone. In addition, the enzymatic rate of the three-enzyme system on QDs, when immobilized on QDs at equal amounts, performed worse than the equivalent free enzyme mixture, clearly highlighting the need for enzyme:QD ratio optimization, and inter-enzyme ratio optimization if working in a multi-enzyme cascade. Altogether, this study demonstrates the enhancement via co-localization of the pathway's enzymes and their relative inter-enzyme distances. They hypothesized that, because the enzymes were tightly packed on the QD surface, the surface itself was unlikely to have an effect on their activity—serving only as a scaffold for co-localization of the enzymes [110]. Critically, since Kang et al. did not report enhancement of single enzymes when immobilized, their study supports a distinct mechanism of enhancement for cascades on QD scaffolds relating to favorable proximity.

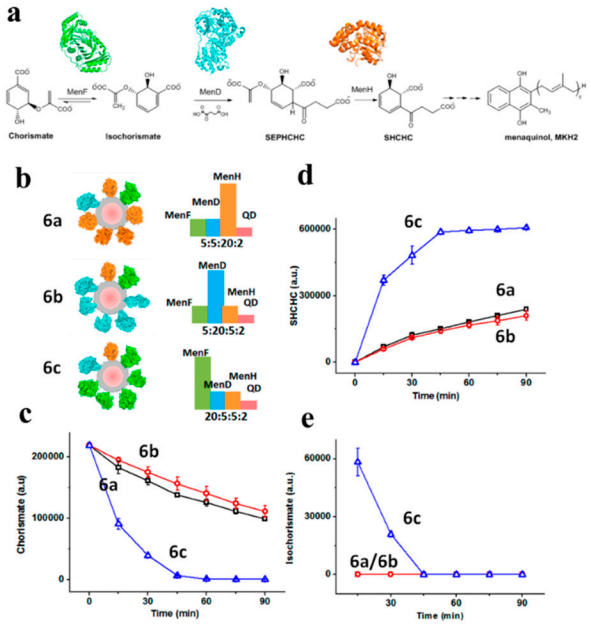

Figure 9. Enhancement of a three-enzyme cascade with QDs. (**a**) Cascade enzymes in the menaquinone synthetic pathway catalyze sequential conversion of chorismate. The structures of MenF, MenD, and MenH were drawn based on their crystal structures (PDB IDs 2EUA, 2JLC, and 2XMZ) and color coded, respectively. Composition of the enzymes in the assemblies drastically affected the catalytic efficacy and intermediate flow. (**b**) Schematic illustration of three multienzyme−QD assemblies with excess MenH (6a), MenD (6b), and MenF (6c), respectively. (**c**) Product (SHCHC) generation catalyzed by

the three assemblies. (**d**) Substrate (chorismate) consumption catalyzed by the three assemblies. (**e**) Intermediate (isochorismate) accumulation catalyzed by the three assemblies. The total amounts of the enzymes and QDs, volumes of the reaction solutions, and the initial concentrations of chorismate were all the same in 6a, 6b, and 6c. Reprinted (adapted) with permission from [110]. Copyright 2018 American Chemical Society, Washington, D.C., USA.

3. Enzyme Immobilization on AuNPs

Similarly to QDs, AuNPs have a high surface area to volume ratio. They have been extensively-studied (see Table 7) in part due to their relatively direct and low-cost, size-tunable synthesis from gold (III) chloride reduction and stabilization (e.g., by citrate). Applications utilizing AuNPs have included chemistry, physics, medicine, and biology. AuNPs have many inherent benefits, including that they can be (1) highly disperse; (2) biocompatible; (3) stable at small scales; (4) synthesized at specific sizes; (5) have a surface plasmon resonance (SPR) band at ~520 nm useful for allowing characterization of sizes, concentration, and binding of molecules; (6) fairly easily (bio)functionalized and stabilized through Au-S bonds, citrate, and non-covalent ionic and hydrophobic interactions; and as NPs have a relatively (7) low cost; (8) are easy to produce; and (9) are environmentally-benign [15,29,51,52,60,61,63] (and refs therein). As mentioned above, enzymes can be immobilized onto AuNPs in a variety of ways. Two of the most common methods for specific conjugation is the use of Ni^{2+}-NTA on the surface of AuNPs to bind to His_6-tagged enzymes, and the use of free cysteines (or free thiol tags) to bind to the AuNP surface. Below, we review a few representative, recent examples of enzyme immobilization onto AuNPs, in addition to the excellent work highlighted in the above section "Factors affecting immobilizing benefits".

Table 7. Overview of representative AuNP-immobilized enzymes.

Nanoparticles/ Nanomaterials	Year	Surface Functionalization	Enzyme Attachment	Enzyme	Multimeric State of the Enzyme	AuNP Diameter (nm)	Enhancement (Compared to Free Enzyme)	Ref
AuNP	2015	MD-Ni^{2+}-AB-NTA	His_6-tag	GPI, GAPDHS, PK	Dimer, Tetramer, Tetramer	5, 10, 20, 50	For GPI: increase k_{cat} and k_{cat}/K_M	[29]
AuNP	2017	None	Adsorption	Horseradish peroxidase	Monomer	10, 20, 30, 40, 60, 80, SS60	None (~lower K_M)	[31]
AuNP	2019	TA-Ni^{2+}-NTA	His_6-tag	PTE	Dimer	1.6, 5.5, 9.9, 20, 55, 100	~10-fold increase k_{cat}, ~2-fold increase k_{cat}/K_M	[76]
AuNP	2012	None, mercapo-alkanoic acid, $(PEG)_n$-carboxylic acid	Adsorption, EDC/NHS crosslinking	Trypsin	Monomer	15, 16.3, 26.7	More stable, less autodegradation, (faster digestion)	[60]
AuNP	2016	HS-PEG_7-COOH	EDC crosslinking	Pepsin	Monomer	31.4	Decrease K_M (73%), increase k_{cat}/K_M (107%), recyclable	[15]
AuNP	2017	None	Adsorption	Pepsin	Monomer	44.1 (DLS), 17.8 (TDA)	Decrease K_M (79%), increase V_{max} (118%), increase k_{cat}/K_M (110%)	[111]
AuNP	2017	Polyelectrolytes [1]	EDC/S-NHS crosslinking	Papain	Monomer	36.4	Decrease K_M (59%), increase V_{max} (143%), increase kcat (4211%), increase k_{cat}/K_M (6667%)	[112]
Fe_3O_4 linked to AuNPs	2013	None (linked to Fe_3SO_4)	Adsorption	Papain	Monomer	55–85	Reusability 5×, 70% retained activity	[52]
Au nanorods	2014	None	Adsorption	Papain	Monomer	~5 × 15 [2]	Increase activity at pH ≥ 9 or temperature ≥ 70 °C, more stable over time	[113]
AuNP	2015	None	Free cysteine (Au-S)	PPase	hexameric	18	None (inhibition)	[114]
AuNP-polymer	2015	None [3]	Free cysteine (Au-S) or absorption	PPase	hexameric	13.1	Increase activity at 50–60 °C but lower than top free activity (45 °C), decrease proteolysis susceptibility	[115]
AuNP polymer	2016	None [4]	Free cysteine (Au-S)	PPase	hexameric	14.2	Decrease proteolysis susceptibility, off/on capability	[116]
Fe_3O_4-AuMNP	2019	Glutathione	Glutaraldehyde	Inulinase [5]	unknown	18.71	Higher temperature stability (>2× at 80 °C) though lower overall, recyclable, increased stability over time	[51]
AuNP	2017	Cysteamine	EDC/NHS crosslinking	Lipase	monomer	25	Decreased KM,app (41%), increased $k_{cat}/K_{M,app}$ (181%), (~3× @ 60 °C) [6]	[63]
AuNP	2019	Unknown [7]	Au-S	Nitroreductase	dimer	50	Decreased K_M (22%), increased k_{cat} (112%), increased k_{cat}/K_M (512%)	[117]
AuNP	2017	DHLA/DHLA-Ni^{2+}-NTA	His_6-tag	PTE (trimer)	Trimer	5, 10, 20	~17-fold increase in V_{max}	[61]

[1] polyelectrolytes included poly(acrylic acid, sodium salt) and poly(allylamine hydrochloride); [2] Roughly estimated from TEM image [3] pNIPAM polymer conjugated to AuNP but not part of enzyme attachment; [4] PMAA and PDMAEMA polymer conjugated to AuNP/polymer but not part of enzyme attachment; [5] 1-ß-$_D$-fructan fructanohydrolase, EC 3.2.1.7; [6] Roughly estimated from figure; [7] AuNP used was 50 nm AuNP 1.5 nM Naked Gold from BioAssay Works, USA, and makeup is proprietary. Abbreviations: AuNP, gold nanoparticle; MD-Ni^{2+}-AB-NTA, mercaptoundecanoic acid EDC/NHS coupled to N,N-bis(carboxymethyl)-$_L$-lysine hydrate loaded with nickel; GPI, glucose-6-phosphate isomerase; GAPDHS, glyceraldehyde-3-phosphate dehydrogenase S; PK, pyruvate kinase; TA-Ni^{2+}-NTA, nitrilotriacetic acid modified thioctic acid loaded with nickel; PTE, phosphotriesterase; PEG, polyethylene glycol; EDC, *N*-(3-dimethylaminopropyl)-*N*′-ethylcarbodiimide hydrochloride; NHS, *N*-hydroxysuccinimide; DLS, dynamic light scattering; TDA, Taylor dispersion analysis; S-NHS, *N*-hydroxysulfosuccinimide sodium; PPase, inorganic pyrophosphatase; Fe_3O_4-AuMNP, gold magnetic nanoparticles; DHLA/DHLA-Ni^{2+}-NTA, 50% dihydrolipoic acid and 50% NTA-appended dihydrolipoic acid loaded with nickel.

Proteases are enzymes that can degrade proteins and peptides, and have been a well-studied enzyme class for immobilization onto NPs. The Lämmerhofer laboratory has completed a series of manuscripts on protease immobilization onto AuNPs, including pepsin, papain, and trypsin [15,60,111,112,118,119]. These could be important for a variety of applications, and have been highlighted by Lämmerhofer and colleagues for sample preparation for liquid chromatography-mass spectrometry (LC-MS) in particular [119]. An early report focused on immobilizing trypsin onto AuNPs [60] (trypsin has been immobilized onto AuNPs in other reports as well, such as in [120]). Immobilization was accomplished using one of two modalities. First, trypsin was immobilized on differently-sized citrate-stabilized AuNPs (~15, 16.3, and 26.7 nm) using adsorption (ionic/hydrophobic interactions). Second, different length spacers of either mercapto-alkanoic acid or mercapto-(PEG)n-carboxylic acid were decorated onto 65 nm AuNPs, giving spacer lengths (number of atoms in final chain) of 3, 4, 12, 16, 17, or 28, in addition to "0" for the adsorption case. These spacers were chemically cross-linked to trypsin using EDC/NHS to couple trypsin amines to the carboxylic acids. The amount of trypsin immobilized onto AuNPs increased with spacer length, approximately plateauing at a spacer length of 16. Overall activity (against a peptide mimic, N_{α}-benzoyl-$_{DL}$-arginine-4-nitroanilide hydrochloride, BApNA) decreased from the adsorption case to the smallest-sized covalent spacer, then increased to about the same level as the adsorption case, but with much more trypsin immobilized on the AuNP, indicating lower activity per enzyme (Figure 10a). The authors also investigated the use of trypsin-AuNP for digestion of three proteins (bovine serum albumin, BSA; cytochrome C, CYC; and myoglobin, MYG) for LC-MS, using differently sized AuNPs and different linkers (Figure 10b). In general, increasing size increased sequence coverage, and the hydrophilic PEG linkers often increased surface coverage more, especially for CYC. Post-optimization, it was found that digestion could also be performed much faster using AuNP-trypsin, with digestion time decreasing from 19 h to ~1 h. It was also found that AuNP-trypsin was generally stable, had less auto-degradation, and could be removed by centrifugation and filtering. This study was significant in demonstrating how to optimize conditions to achieve these desirable benefits to the enzyme via immobilization.

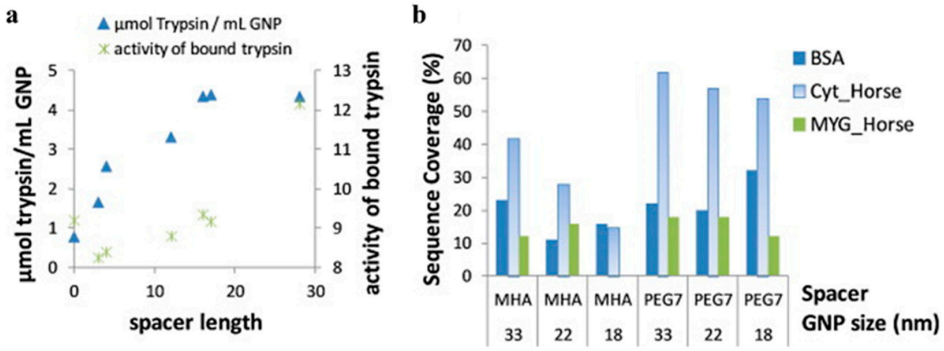

Figure 10. Influence of spacer length on immobilization chemistry and bioactivity. (**a**) With increase of immobilized enzymes (blue) an increase of the enzyme activity (ΔA_{410nm} min^{-1}) in the supernatant could be observed as well measured with N_{α}-Benzoyl-DL-arginine 4-nitroanilide hydrochloride (BApNA) assay (green). (**b**) The right figure shows the sequence coverage (%) of the MASCOT search result for the digested proteins albumin, cytochrome C and myoglobin as a function of GNP size (33 nm, 22 nm and 18 nm according to dynamic light scattering—DLS, measurement) and of spacer length (MHA, mercaptohexadecanoic acid, spacer length: 17 atoms; PEG7, O-(2-carboxyethyl)-O'-(2-mercaptoethyl) heptaethylene glycol, spacer length: 28 atoms). Reproduced with permission from [60]. Copyright 2012, Elsevier B.V., Amsterdam, Netherlands.

The Lämmerhofer laboratory has published additional articles relating to proteases on AuNPs, summarized here. Pepsin was immobilized onto AuNPs coated with HS-PEG7-COOH using EDC coupling [15]. The final AuNP-PEG7-pepsin had a greater diameter by DLS (105.3 nm) than the

AuNP-PEG7 (52.1 nm) or the AuNP-citrate (31.4 nm); for comparison, AuNP-citrate-pepsin by adsorption (66.5 nm) and pepsin alone (3.9 nm) were also smaller. Pepsin on AuNP had a final concentration of 7.24 μM. For the cleavage of CYC, AuNP-pepsin compared to free pepsin had a smaller K_M (73%), V_{max} (78%), and k_{cat} (78%) to give an ultimately higher K_{cat}/K_M (107%) as compared to unconjugated enzyme. The AuNP-pepsin could also be recycled multiple times, although score and sequence coverage decreased. Follow-up work developed an assay using amino acid analysis to quantitate the amount of pepsin adsorbed onto AuNPs [118]. Further work investigated other methods to characterize AuNP-pepsin [111]. Here, pepsin adsorbed onto 44.1 nm citrate-stabilized AuNP gave diameters of ~64 nm average by DLS (one outlier of 79.7 nm). Multiple methods were utilized to examine pepsin surface coverage of AuNPs. Lowry assay of the supernatant (i.e., calculating amount not bound to AuNP) gave 16,002–314,673 pepsins per AuNP depending on the amount of pepsin added. Resonance mass measurement using a microfluidic system to measure the buoyant mass of the pepsin-AuNP gave a direct measurement of surface coverage. From this measurement, it was found that: (1) a population of AuNPs were either unmodified or had low surface coverage; and (2) for a specific treatment of AuNP, there were 73,513 pepsins per AuNP on average (compared to 51,745 pepsins per AuNP by the Lowry assay for similar conditions). Taylor dispersion analysis (TDA) was used to more accurately determine size differences of the pepsin-AuNPs produced from different amounts of added pepsin. From this analysis, the diameter of the pepsin-AuNP ranged from 17.0 to 23.7 nm, and the calculated surface coverage was 47,321–128,219 pepsins per AuNP. A binding isotherm indicated that the effective dissociation constant was 30.7 ± 4.1 μM. Finally, the bioactivity was compared between free pepsin, adsorbed pepsin on AuNPs, and covalently-bound pepsin on AuNPs (amide coupling with PEG spacer as in [15]). Relative to free pepsin, K_M and k_{cat} decreased for both immobilized samples, while k_{cat}/K_M increased (Table 8).

Table 8. Comparison of kinetic data for digestion of cytochrome C as model protein.

Parameter	Free Pepsin [1]	Adsorbed Pepsin-AuNP	Covalent Pepsin-AuNP [1]
K_M [M]	$(2.93 \pm 0.29)\cdot10^{-5}$	$(2.32 \pm 0.15)\cdot10^{-5}$ (79%)	$(2.14 \pm 0.15)\cdot10^{-5}$ (73%)
V_{max} [M s^{-1}]	$(4.44 \pm 0.30)\cdot10^{-8}$	$(5.23 \pm 0.36)\cdot10^{-8}$ (118%)	$(3.47 \pm 0.22)\cdot10^{-8}$ (78%)
k_{cat} [s^{-1}]	$(6.13 \pm 0.41)\cdot10^{-3}$	$(4.62 \pm 0.32)\cdot10^{-3}$ (75%)	$(4.79 \pm 0.31)\cdot10^{-3}$ (78%)
k_{cat}/K_M (M^{-1} s^{-1})	$(2.09 \pm 0.12)\cdot10^{+2}$	$(2.29 \pm 0.16)\cdot10^{+2}$ (110%)	$(2.24 \pm 0.02)\cdot10^{+2}$ (107%)

Digestion was by free pepsin (Free Pepsin), adsorptively bound pepsin-AuNP (Adsorbed Pepsin-AuNP), and covalently-linked pepsin-AuNP (Covalent Pepsin-AuNP). Percentages in parentheses are values relative to free pepsin. Adapted with permission from ref. [111]. Copyright 2017 Elsevier B.V. [1] Within this table, free pepsin data were taken from Höldrich et al. (2016), ref [15]. Copyright 2016 Springer-Verlag Berlin Heidelberg, Germany.

Finally, the Lämmerhofer laboratory also investigated papain immobilized on AuNPs [112]. In this case, the authors started with citrate-stabilized AuNPs and then used a layer-by-layer process to add on the polyelectrolytes poly (allylamine hydrochloride) (PAH; Mw. ~17,500; cationic) and poly (acrylic acid, sodium salt) (PAA; Mw. ~15,000; anionic) for (1) increased colloidal stability and (2) multiple anchor groups for covalently-attaching papain using EDC/sulfo-NHS amine coupling between polyelectrolyte carboxylic acids and papain amines (sulfo-NHS, *N*-hydroxysulfosuccinimide sodium). The authors note that immobilization on the first-layered AuNP-PAH failed due to aggregation in phosphate buffer. DLS measurements indicated that the diameter of the citrate-AuNP (36.4 nm) increased with PAH (127.6 nm), stayed similar with addition of PAA (126.3 nm for AuNP-PAH-PAA), and then increased with increasing concentrations of papain added for immobilization (176.2–1314.7 nm). Resonant mass measurement was used to determine the surface coverage and concentration of AuNPs. For 0.2 mg mL^{-1} added papain, ~23,900 bound to each AuNP; for 1 mg mL^{-1} added papain (~5× increase), this jumped to ~2,060,000 (~100× increase). The authors speculated this was due to conformational arrangement and morphology. The authors also note that given the calculated surface area of the AuNP, it is likely that there is multilayer binding of the papain to the AuNPs. The peptide mimic BApNA was again used for activity measurements (vide supra). In this case, immobilization was striking in its

enhancement of papain activity (Table 9). This enhancement can save significant amounts of enzyme. As the authors note, in the preparation of papain-AuNP using 1 mg mL^{-1} papain, only 21.3 μg mL^{-1} is conjugated (the rest could be recycled); yet, this smaller amount of enzyme (1/0.0213 = ~47× less) still produces a higher V_{max} than free papain (143% increase, Table 9, for a total "savings" of ~67× of enzyme. In terms of applications, the authors show that papain-AuNPs can cleave IgG (for LC-MS analysis) and that papain does not bleed off from the AuNP to interfere with analysis.

Table 9. Summary of the kinetic parameters (K_M, V_{max}, k_{cat}) calculated for both free papain and immobilized papain.

Parameter	Free Papain [1]	Papain-AuNP [2]
K_M [mM]	2.71 ± 0.98	1.61 ± 0.03 (59%)
V_{max} [mM s^{-1}]	(2.03 ± 0.57)·10^{-4}	(2.91 ± 0.03)·10^{-4} (143%)
k_{cat} [s^{-1}]	(4.75 ± 1.33)·10^{-3}	0.20 ± 0.02 (4211%)
k_{cat}/K_M (mM^{-1} s^{-1})	(1.8 ± 0.2)·10^{-3}	0.12 ± 0.03 (6667%)

Values represent mean ± standard deviation of three replicate experiments. Adapted with permission from ref. [112]. Copyright 2017 Elsevier B.V., Amsterdam, Netherlands [1] The final papain concentration in the digestion solution was 1 mg mL^{-1} (at a Mw. of 23,406 Da this is ~42.7 μM). [2] The papain concentration used for immobilization was 1 mg mL^{-1}; however, the final concentration in the digestion solution was 1.48 μM, or ~28.9× less concentrated than free papain.

In regards to papain immobilization, Sahoo et al. and Homaei et al. examined immobilization using other gold-associated nanocomposites [52,113]. Sahoo et al. used magnetic Fe_3O_4 NP surrounded by linkers that ultimately chemisorbed to citrate-stabilized AuNPs (which they termed magnetic gold nanocomposites) which then had papain adsorbed [52]. The magnetic gold nanocomposites had a diameter of 55–85 nm. Importantly, the immobilized papain could be separated with a magnet, washed, and reused up to 5 times while maintaining 70% of its initial catalytic activity. Homaei et al. used gold nanorods with adsorbed papain and measured casein hydrolysis [113]. The immobilized papain tended to show slightly lower activity overall, but showed considerably higher activity at pH ≥ 9 and temperatures ≥70 °C. The greatest benefit was seen in stability, with the immobilized papain being considerably more stable over time (Figure 11), and less sensitive to inhibition by selected metal ions.

In addition to proteases, other enzymes have been immobilized on AuNPs, including pyrophosphatase (PPase). PPase is an important recycling enzyme responsible for hydrolyzing pyrophosphate (PPi) into inorganic phosphate (Pi). A series of papers by the Chen and Yuan laboratories have explored immobilization of PPase on AuNPs with and without organic polymers [114–116,121]. In Liu et al., the authors investigated the effects of orientation and surface density on PPase activity when bound to an ~18 nm diameter AuNP (Figure 12a) [114]. Three types of PPase were used: wild-type (WT) which bound by adsorption; MT1, which was mutated to have a free cysteine near the active site to bind the AuNP; and MT2, which was mutated to have a free cysteine away from the active site. The authors also added different amounts of PPase to the AuNP to modulate surface density; upon protein binding the diameter increased by ~3–4 nm. In general, MT1 and MT2 has somewhat higher amounts bound to the AuNP than WT. All enzymes lost activity compared to free PPase ("relative activity"), but MT2 was the most active of the bound PPase enzymes, indicating orientation was important (Figure 12b). Increased surface density also improved activity, but generally to a lesser degree (Figure 12b).

Following up on this work, in another publication Liu et al. added a temperature-responsive polymer with a free thiol, poly(*N*-isopropylacrylamide) or pNIPAM, to an AuNP with PPase [115]. The goal was to modulate PPase activity dependent on temperature. When the temperature increases above a reversible lower critical solution temperature or LCST (~32 °C), pNIPAM goes from an extended hydrophilic state to a collapsed hydrophobic state (Figure 12c). In theory, when extended, the polymer would sterically block the bound PPase, but when the temperature increased and the polymer shrunk

the PPase would be exposed for activity. The size of the construct increased from 13.1 nm for the AuNP, to 15.5 with PPase (~58 PPase/AuNP, leaving free space for pNIPAM), to 24.1 nm with pNIPAM additionally added, and then decreased to 18.1 nm when the temperature was raised from 25 °C to 45 °C (AuNP-pNIPAM alone was 27.1 nm). Since the Au-S bound is unstable at >60 °C, only temperatures ≤60 °C were investigated. It was found that at 25 °C, the activity of AuNP-PPase-pNIPAM was only 46.4% of free PPase at 25 °C, but as temperature increased to 50 °C and the polymer collapsed exposing the enzyme, the activity jumped to 110% of free PPase at 50 °C, an increase of 280% for the AuNP-PPase-pNIPAM (Figure 12d). The authors optimized the system and found that for the conditions they tried, a 10 kDa pNIPAM worked best for off/on switching, a ratio of 1.4:1 PPase: pNIPAM was best on the AuNP, and orientation using a mutated PPase with a free cysteine away from the active site worked best. Finally, the authors also showed that a benefit of the polymer was protection from proteolysis: upon treatment with trypsin for 90 min, the relative specific activity for free PPase dropped by ~50% and 70% at 25 °C and 45 °C, respectively, while AuNP-PPase-pNIPAM activity dropped by only ~25 and 30% respectively.

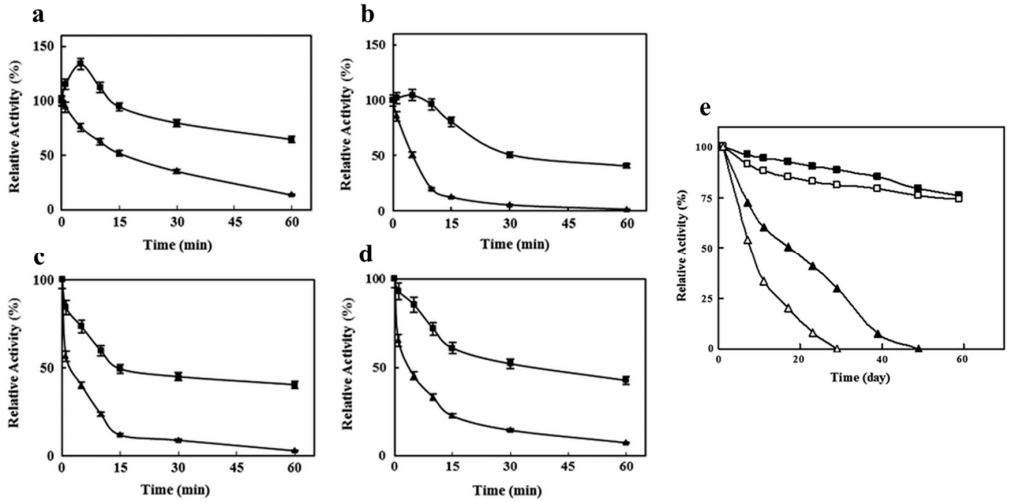

Figure 11. Stability of free papain (triangles) and papain immobilized on gold nanorods (squares) in mixed buffer. (**a**) Irreversible thermoinactivation at 80 °C. (**b**) Irreversible thermoinactivation at 90 °C. (**c**) Enzyme stability at pH 3.0. (**d**) Enzyme stability at pH 12.0. Native and linked papain were incubated at the different above-reported experimental conditions then aliquots of the enzyme were withdrawn at different times, cooled on ice, adjusted at pH 9.0 and the residual activity measured under the assay conditions in substrate saturation conditions. Control data were obtained measuring the activity of the same stock of enzyme solution kept for the same times on ice for thermal and at room temperature for the pH stability experiments. (**e**) Storage stability of free and immobilized papain at 4 °C (solid) and 22 °C (hollow). Measurements were carried out in substrate saturation conditions. Reproduced with permission from ref. [113]. Copyright 2014 Springer-Verlag. Wien, Austria.

Building on this work, two other polymers were used instead to give AuNP-PPase pH responsiveness [116] (Figure 12e). To a 14.2 nm diameter AuNP was added PPase to give the 18.4 nm diameter AuNP-PPase. To this was added the polymer poly (methacrylic acid) or PMAA with a free thiol to bind to the AuNP for a diameter of 35.1 nm. This polymer has carboxylic acid groups and therefore at pH 7–9 is mostly negatively charged. To this was added the polymer poly(2-(dimethylamino)ethyl methacrylate or PDMAEMA. This polymer has a pK_a between 7.5 and 8, so that at pH 7 it is positively charged, binds to the negatively-charged AuNP-PPase-PMAA, decreasing surface charge of the complex leading to instability and aggregates with a diameter of 560 nM. Conversely, at pH 9 PDMAEMA is near neutral and can dissociate, allowing AuNP-PPase-PMAA to disperse (diameter of 41.7 nm). This leads to a drop of relative activity at pH 7 of 16.9% ("off") and an increase to 97.9% at pH 9 ("on") (Figure 12f). The authors found that from their conditions

tested, a PMAA of 19.9 kDa and a feed ratio of 150:1 for PPase:AuNP with a 14 nm diameter was best for modulating activity. Importantly, this system could be cycled multiple times, *albeit* with a slight decrease in overall activity with each cycle perhaps due to irreversible aggregation of a small amount of AuNPs. The system was also able to protect PPase from trypsin digestion: after 90 min, the relative activity was ~40% for free PPase, ~50% for AuNP-PPase, ~60% for AuNP-PPase-PMAA, and 86.4% for AuNP-PPase-PMAA/PDMAEMA, or ~2× that of free PPase (pH 7 for 90 min of trypsin treatment then pH 9 for activity reading). Finally, Li et al. extended this system to a surface for pH responsive capture and release [121]. PDMAEMA was bound to AuNP layers, and was used to bind AuNP-PPase-PMAA at pH 7 and release it at pH 10, and this could be cycled on and off. Horseradish peroxidase (HRP) bound to AuNP was also used, to demonstrate that (1) AuNP-PPase-PMAA could be bound then released from the surface, followed by binding of AuNP-HRP-PMAA and release, and (2) AuNP-PPase-PMAA and AuNP-HRP-PMAA could be bound to the surface simultaneously.

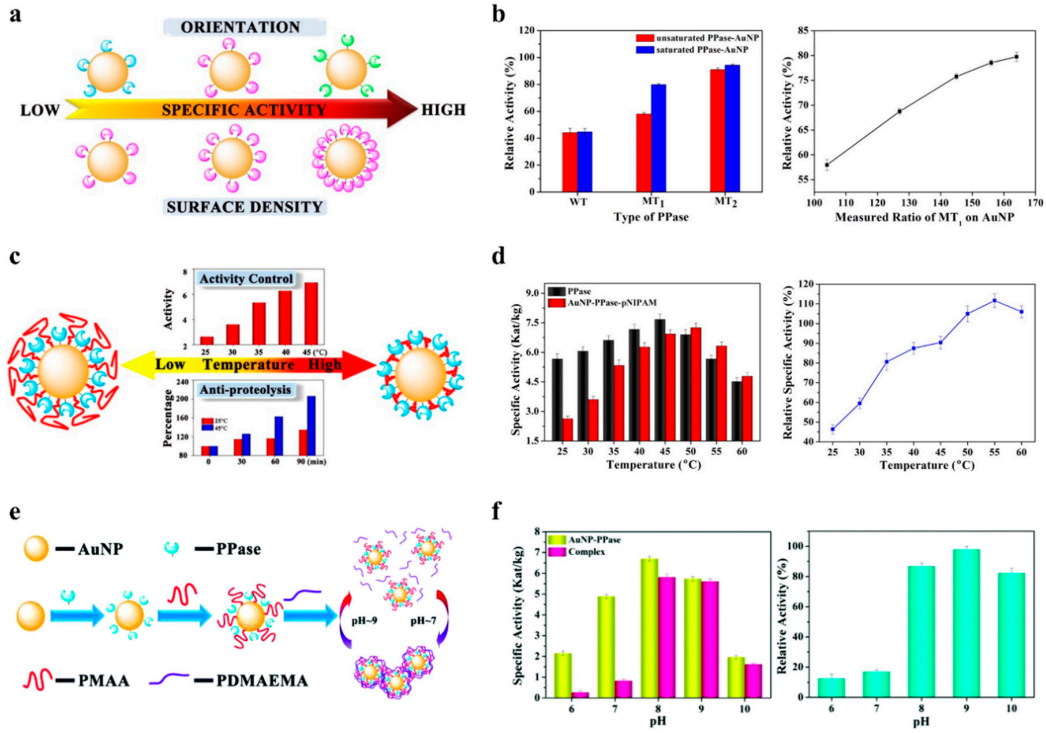

Figure 12. Pyrophosphatase (PPase) immobilized on AuNPs (**a**) Overview of investigation of PPase activity in relation to orientation and surface density on AuNPs, (**b**) (Left) Relative activity of PPase bound to AuNP under unsaturated conditions (PPase/AuNP molar ratio in the feed was 60) and saturated conditions (PPase/AuNP molar ratio in the feed was 400), (Right) Relative specific activity of MT_1 bound to AuNP as a function of the feed composition. (**a**,**b**) Abbreviations: WT, wild-type; MT_1, mutant with cysteine near active site; MT_2, mutant with cysteine far from active site. Reproduced with permission from ref. [114]. Copyright 2015 American Chemical Society, Washington, DC, USA. (**c**) Overview of investigation of PPase activity and proteolysis protection in relation to polymer extension on AuNP, (**d**) (Left) Specific activity of native PPase and the conjugates at different temperatures (±SD, n = 3), (Right) relative specific activity of the conjugates (compared with the native PPase) at different temperatures (±SD, n = 3). (**c**,**d**) Abbreviations: pNIPAM, poly(*N*-isopropylacrylamide). Reproduced with permission from ref. [115]. Copyright 2015 American Chemical Society, Washington, DC, USA. (**e**) Overview of investigation of PPase activity in relation to PDMAEMA polymer off/on attachment due to pH, (**f**) (Left) Specific activity of AuNP–PPase and AuNP–PPase–PMAA/PDMAEMA complexes at different pH values (±SD, n = 3), (Right) relative specific activity of the AuNP–PPase–PMAA/PDMAEMA complex (compared with AuNP–PPase) at different pH values (±SD, n = 3). (**e**,**f**) Abbreviations: PMAA, (poly)methacrylic acid; PDMAEMA, poly(2-(dimethylamino)ethyl methacrylate. Reproduced with permission from ref. [116]. Copyright 2016 The Royal Society of Chemistry, London, United Kingdom.

In addition to the above referenced papers, a few more examples are worth mentioning. In Mohammadi et al., the enzyme inulinase, which hydrolyzes fructose-containing polymers and inulin, was investigated [51]. Magnetic iron NPs were made, and mixed with gold to produce Fe_3O_4-Au magnetic NPs, which were capped with glutathione (18.71 nm diameter). Glutaraldehyde was then used to immobilize inulinase onto the NPs (22.95 nm diameter). Enzyme activity after immobilization was 83%. The immobilized inulinase had a higher K_M (6.8 vs. 5.4 mg mL^{-1}), a lower V_{max} (3.03 vs. 3.55 μmol min^{-1} mL^{-1}), a lower k_{cat} (841.67 vs. 986.11 min^{-1}), and a lower k_{cat}/K_M (123.77 vs. 182.61 min^{-1} mg^{-1} mL). However, the immobilized inulinase had higher temperature stability, keeping >80% of the relative activity vs. <40% for free inulinase at 80 °C. Importantly, the authors state that the food industry prefers reactions at higher temperature because of increased inulin solubility, lower microbial contamination, and better rates. Both free and immobilized inulinase kept ca. the same relative activity over 8 h at 50 °C and 60 °C. Importantly, the immobilized inulinase could be recycled after separation from the reaction mixture by a magnetic field up to 10 times while maintaining >70% relative activity. Finally, the stability of immobilized inulinase at 28 °C after 45 days (73% remaining relative activity) was higher than free inulinase (31% remaining relative activity).

Shikha et al. also investigated the heat stability of an immobilized enzyme, in this case lipase [63]. AuNP was capped with cysteamine (25 nm diameter) and linked to lipase using EDC/NHS. The immobilized lipase had a lower apparent K_M (2.76 vs. 6.70 mM), a lower V_{max} (3.71 vs. 4.98 U μg^{-1} protein), a lower k_{cat} (2059.05 vs. 2763.30 s^{-1}), and a greater $k_{cat}/K_{M,\,app}$ (744.95 vs. 412.38 s^{-1} mM^{-1}). While enzyme activity of free lipase over the range of 20–80 °C was generally higher than or similar to immobilized lipase, at 60 °C the activity of the immobilized lipase (65% of maximum) was significantly higher than free lipase (~20% maximum activity). This was also shown through a temperature sensitivity assay over 10 h, where the immobilized lipase retained more activity than the free lipase at 40, 50, and 60 °C; after 4h, the immobilized lipase still had >50% relative activity at 40 and 50 °C whereas free lipase relative activity was ~30%.

In an interesting application, Ball et al. used a nitroreductase (NfnB) with an engineered histidine and cysteine tag (NfnB-cys) immobilized on an AuNP to activate the prodrug 5-(aziridin-1-yl)-2,4-dinitrobenzamide (CB1954) for potential application in Directed Enzyme Prodrug Therapy (DEPT) for cancer treatment [117]. The prodrug has two nitro groups at the 2 and 4 positions that can be reduced to NHOH. The authors found different 2-NHOH:4-NHOH product ratios for free NfnB-his tag (44:56), free NfnB-cys (32:68), and the immobilized NfnB-cys (13:87). At least for the free NfnB-his tag and free NfnB-cys, this was due to differences in rates of further non-enzymatic reduction to 2-NH2:4-NH2 and the rate of the enzymes before HPLC analysis. In terms of activity, the immobilized NfnB-cys vs. the free NfnB-cys had a lower K_M (1108.67 vs. 5078.37 μM), a lower V_{max} (10.89 vs. 19.37 μM s^{-1}), a higher k_{cat} (61.85 vs. 55.34 s^{-1}) and a higher k_{cat}/K_M (0.0558 vs. 0.0109 μM^{-1} s^{-1}).

Finally, in another example of an enzyme conjugated onto AuNPs, Hondred et al. examined a trimer of PTE conjugated to 5, 10, and 20 nm AuNPs [61]. The PTE trimer was constructed by each monomer containing PTE, a collagen-like triple helix domain, a trimerization domain, and a His_6 tag, and being allowed to trimerize [82]. The His_6-tags could then bind a DHLA-Ni^{2+}-NTA coated AuNP. Conjugation onto the 20 nm AuNP resulted in the highest average turnover increase over free PTE trimer (~ 1.7× over 10 nm AuNPs; ~1.1× over 5 nm AuNPs) when holding the concentration of AuNPs constant and varying the amount of PTE trimer displayed. Relative enzyme efficiency (k_{cat}/K_M) over free PTE trimer was highest with the 10 nm AuNP in the fixed AuNP concentration method (~ 3.0×), but was highest with the 5 nm AuNP for a fixed PTE trimer concentration method (5.0×). Overall, the V_{max} was increased by ~17× using 20 nm AuNP at low PTE trimer concentration (5 pM) and at a low enzyme:scaffold ratio (1:1).

4. Discussion—Conclusions, Outlook, and Perspective

Enzymes are active accelerators of many biochemical processes and are widely used to catalyze reactions in a wide array of biological and industrial applications. NPs have been shown to enhance

the effectiveness of immobilized enzymes, which has driven research interest in NP–enzyme systems. Although not all NP–enzyme conjugates have demonstrated an increase in enzymatic activity, many have, as described above. Among NPs, QDs and AuNPs are of particular popularity, potentially due to many of their shared properties owing to their being nanocrystalline, predominantly monodispersed, with certain favorable properties, including size-tunable photoluminescence and the capacity to act as excellent FRET donors and acceptors, in the case of QDs, and surface plasmon resonance for AuNPs [90].

As can be seen with several representative examples presented in this review, while NP-associated enhancement is still not entirely predictable and additional research is required, the existing literature can provide a solid basis for a grasp of how enzymatic activity is enhanced in NP systems and for NP–enzyme system design. Here, in every case we covered, the NP acts as the central nano-scale scaffold for displaying the enzyme, which in turn reflects that NP quality, surface functionalization approaches for aqueous dispersal, and the chemistries to attach the enzymes and/or substrates to the NP are critically important for enzymatic activity. Especially since QDs and AuNPs are metallic in nature, they display no inherent solubility in water and must thus be stabilized as colloids through the addition of surface ligands to their surface, which can greatly impact enzymatic activity.

Other NP-related aspects such as NP size and enzyme:NP ratio were closely examined and discussed in detail. Investigation of each NP's size, curvature, and morphology offer a better understanding of the enhancement of activity of enzymes immobilized on NPs and can be further investigated to optimize the design of new NP–enzyme systems for various biological and industrial applications. Furthermore, enzyme:NP ratio has a significant impact on enzymatic activity—either positive or negative. Recent work and an initial meta-analysis of available work with reported kinetic parameters suggests the hypothesis of a "sweet-spot" consisting of both a small diameter NP with fairly low enzyme coverage, consistent with low enzyme: NP ratios [19,22,39,81,82]. Possible explanations are that this could be due to a relief of ligand crowding with an increase in curvature (and decrease in diameter) as a result of released steric hindrance or an increase in product solubility in the NP hydration layer which could also help with product partitioning or release. Nevertheless, with greater accumulation of work reporting the impact of NP attributes on kinetic parameters of enzymes they are immobilized to will significantly improve the confidence in the "sweet spot" hypothesis and other related trends which may allow for the better utilization of modeling or generation of design rules for NP–enzyme systems for optimal performance. In addition, future work will likely assist in determining whether NP immobilization of enzymes is cost-effective.

One can expand this into a cost–benefit analysis by determining the relative complete turnover rates for each sample immobilized vs. free in solution (Tables 4 and 5, last two columns, as well as Appendix A Table A3). Does it make sense to use AuNP immobilization? One can determine this from the last column ((Extra) PTE per AuNP); as long as the cost ratio of the NP to PTE exceeds this value, it is more economical to use immobilization. For illustration, using the 32:1 PTE:AuNP conjugate data from Table 4, if a mole of PTE costs \$1, as long as a mole of NP costs <\$111.8, it is more economical to immobilize. From Table 5, one can see that the cost ratio is even more beneficial for larger AuNPs at low coverage (i.e., the 100 nm AuNP can cost up to 2103.5× the cost of PTE, mol/mol). Which size AuNP and what percentage coverage makes the most sense to use will depend on the relative costs. For example, using the data from Table 4, 5.9 of the most efficient 4:1 PTE:AuNP conjugates (=23.6 PTE total) gives the same approximate overall turnovers (5.9 × 4 × 79.2 = 1869 turnovers) as 1 of the 32:1 PTE:AuNP conjugates (=32 PTE total; 32 × 58.4 = 1869 turnovers), gaining ~8.4 "extra" PTEs at the cost of 4.9 more AuNPs. Dividing this out, if a mole of AuNPs costs <1.72× the cost of a mole of PTE, then low coverage (4:1) is better; otherwise, higher coverage (32:1) is better. As another example, using the data from Table 5, 45.5 of the most efficient 10 nm PTE:AuNP conjugates (=273.1 PTE total) gives the same approximate overall turnovers (45.5 × 6 × 81.2 = 22,168 turnovers) as 1 of the 100 nm PTE:AuNP conjugates (=601 PTE total; 601 × 36.9 = 22,177), gaining ~327.9 "extra" PTEs at the cost of 44.5 more AuNPs. Dividing this out, if a mole of 10 nm AuNPs costs <7.37× the

cost of a mole of PTE, then the smaller conjugate (10 nm) is better; otherwise, the larger conjugate (100 nm) is better (this is before considering that the 100 nm conjugate likely costs more than the 10 nm conjugate). Of course, the degree of benefit to enzymes will change depending on enzyme; this example illustrates the importance of trying conjugates at different enzyme:scaffold ratios (this becomes even more important with multienzyme cascades and investigating the ratios between enzymes as well as between each enzyme and the scaffold). Beyond the interest from the perspective of fundamental science, the reviewed literature suggests significantly less enzyme could be used to accomplish the same levels of activity and/or product production, when displayed on the surface of a NP, which may greatly inspire industrial applications and for usage in other applications, including cell-free synthetic biology systems, where a modular scaffold for any cascaded enzymatic system could greatly improve the state of cell-free synthesis.

Supplementary Materials: The following are available online at http://www.mdpi.com/2073-4344/10/1/83/s1, Table S1: The relationship between fold-change in k_{cat} as a function of QD and AuNP diameter and enzyme:NP ratio.

Author Contributions: All aspects of this review were conducted by all authors: G.A.E., S.N.D., S.A.W., and I.L.M. All authors have read and agreed to the published version of the manuscript.

Funding: This research was funded by support from NRL Base 6.1 funds, the NRL Nanoscience Institute, the National Institute of Food and Agriculture, U.S. Department of Agriculture, under award number 11901762, and by the U.S. Assistant Secretary of Defense for Research and Engineering (ASD(R&E)) through the Applied Research for Advancement of S&T Priorities Synthetic Biology for Military Environments program.

Conflicts of Interest: The authors declare no conflict of interest. The funders had no role in the design of the study; in the collection, analyses, or interpretation of data; in the writing of the manuscript, or in the decision to publish the results.

Appendix A

Table A1. Analysis of averaged enzyme activities for fixed NP diameter format on 10 nm AuNPs.

"A"	"B"	"C"	"D"	"E"	"F"	"G"	"H"	"I"	"J"
PTE: AuNP	**Turnovers per PTE-AuNP (s^{-1})**	**#PTE^{free} to equal PTE-AuNP**	**(Extra) PTE per AuNP**	**AuNP volume (nm^3) [1]**	**(Extra) PTE per AuNP nm^3**	**Additional (PTE-AuNP)s to equal (32:1 PTE:AuNP total turnovers)**	**Total #PTE to equal (32 PTE:AuNP total turnovers)**	**(Extra) PTE over 32:1 PTE:AuNP**	**[(Extra) PTE/(Extra) AuNP] to equal 32:1 PTE:AuNP**
-	(k_{cat}) * ("**A**")	("**B**")/(k_{cat} of free PTE)	("**C**")—("**A**")	(4/3) * π * (5 nm)^3	("**D**")/("**E**")	["**B**" for 32 PTE:AuNP)/("**B**")]—1	["**G**") + 1] * ("**A**")	32—("**H**")	("**I**")/("**G**")
1	61.9	4.8	3.8	523.60	0.007	29.2	30.2	1.8	0.06
2	152.2	11.7	9.7	523.60	0.019	11.3	24.6	7.4	0.66
4	316.8	24.4	20.4	523.60	0.039	4.9	23.6	8.4	1.72
8	537.6	41.4	33.4	523.60	0.064	2.5	27.8	4.2	1.69
16	880	67.7	51.7	523.60	0.099	1.1	34.0	−2.0	−1.76
32	1868.8	143.8	111.8	523.60	0.213	0.0	32.0	0.0	NA

Calculations for Table 4, based on data from Breger et al. First row denotes columns for reference. Second row denotes column titles. Third row denotes calculations. [1] Based on nominal diameter of 10 nm (by TEM, 9.9 nm). "PTE:AuNP" is the approximate ratio of PTE to AuNP; "Turnovers per PTE-AuNP (s^{-1})" is the number of turnovers for each PTE-AuNP; "#PTE^{free} to equal PTE-AuNP" is the number of free PTEs that would be required to match the PTE-AuNP's k_{cat}, calculated using the PTE free k_{cat} in Table 4. "(Extra) PTE per AuNP" is the number of relative free PTEs gained by using PTE-AuNP. "AuNP volume (nm^3)" is the estimated spherical volume of a 10 nm AuNP. "(Extra) PTE per AuNP nm^3" is the number of relative free PTEs gained by using PTE-AuNP per each nm^3 of AuNP volume. Dashed line represents start of analysis comparing PTE:AuNPs to 32:1 PTE:AuNP. "Additional (PTE-AuNP)s to equal (32 PTE:AuNP total turnovers)" is the number of additional PTE-AuNP at each ratio needed to equal the total turnovers of one 32 PTE:AuNP conjugate. "Total #PTE to equal (32 PTE:AuNP total turnovers)" is the number of PTEs needed to equal the total turnovers of one 32:1 PTE:AuNP conjugate. "(Extra) PTE over 32 PTE:AuNP" is the number of PTEs saved by using multiple PTE-AuNPs of lower ratio vs. one PTE-AuNP at 32:1 PTE:AuNP. "[(Extra) PTE/(Extra) AuNP] to equal 32:1 PTE:AuNP" is the number of PTEs saved by using multiple PTE-AuNPs of lower ratio vs. one PTE-AuNP at 32:1 PTE:AuNP over the number of extra AuNPs required for those multiple PTE-AuNPs. Error ranges removed for clarity but are in referenced publication. Initial values draw from Breger et al., and utilized for subsequent analysis here [76].

Table A2. Averaged enzyme activities for fixed enzyme density format for low coverage conditions.

"A"	"B"	"C"	"D"	"E"	"F"	"G"	"H"	"I"	"J"	"K"
AuNP Dia. (nm)	**PTE: AuNP**	**Turnovers per PTE-AuNP (s^{-1})**	**#PTE^{free} to Equal PTE-AuNP**	**(Extra) PTE per AuNP**	**AuNP Volume (nm^3) [1]**	**(Extra) PTE per AuNP nm^3**	**Additional (PTE-AuNP)s to Equal (601:1 PTE:AuNP Total Turnovers)**	**Total #PTE to Equal (601 PTE:AuNP Total Turnovers)**	**(Extra) PTE over 601:1 PTE:AuNP**	**[(Extra) PTE/(Extra) AuNP] to Equal 601:1 PTE:AuNP**
—	—	(k_{cat}) * ("**B**")	("**C**")/(k_{cat} of free PTE)	("**D**")—("**B**")	(4/3) * π * ("**A**"/2 nm)^3	("**E**")/("**F**")	["**C**" for 601 PTE:AuNP)/("**C**")]—1	[("**H**") + 1] * ("**B**")	601—("**I**")	("**J**")/("**H**")
1.5	1.25	73.9	9.0	7.8	1.77	4.391	299.2	375.2	225.8	0.75
5	1.5	170.0	13.0	11.5	65.45	0.176	206.4	311.0	290.0	1.41
10	6	487.2	59.4	53.4	523.60	0.102	44.5	273.1	327.9	7.37
20	24	1416.0	172.7	148.7	4188.79	0.035	14.7	375.9	225.1	15.35
55	182	9882.6	1205.2	1023.2	87,113.75	0.012	1.2	408.4	192.6	154.81
100	601	22176.9	2704.5	2103.5	523,598.78	0.004	0.0	601.0	0.0	NA

Calculations for Table 5, based on data from Breger et al. First row denotes columns for reference. Second row denotes column titles. Third row denotes calculations. [1] Based on nominal diameters (similar to those by TEM). "AuNP dia. (nm)" is the nominal diameter of the AuNP. "PTE:AuNP" is the approximate ratio of PTE to AuNP; "Turnovers per PTE-AuNP (s^{-1})" is the number of turnovers for each PTE-AuNP; "#PTE^{free} to equal PTE-AuNP" is the number of free PTEs that would be required to match the PTE-AuNP's k_{cat}, calculated using the PTE free k_{cat} in Table 4. "(Extra) PTE per AuNP" is the number of relative free PTEs gained by using PTE-AuNP. "AuNP volume (nm^3)" is the estimated spherical volume of a 10 nm AuNP. "(Extra) PTE per AuNP nm3" is the number of relative free PTEs gained by using PTE-AuNP per each nm^3 of AuNP volume. Dashed line represents start of analysis comparing PTE:AuNPs to 601:1 PTE:AuNP. "Additional (PTE-AuNP)s to equal (601 PTE:AuNP total turnovers)" is the number of additional PTE-AuNP at each ratio needed to equal the total turnovers of one 601 PTE:AuNP conjugate. "Total #PTE to equal (601 PTE:AuNP total turnovers)" is the number of PTEs needed to equal the total turnovers of one 601:1 PTE:AuNP conjugate. "(Extra) PTE over 601 PTE:AuNP" is the number of PTEs saved by using multiple PTE-AuNPs of lower ratio vs. one PTE-AuNP at 601:1 PTE:AuNP. "[(Extra) PTE/(Extra) AuNP] to equal 601:1 PTE:AuNP" is the number of PTEs saved by using multiple PTE-AuNPs of lower ratio vs. one PTE-AuNP at 601:1 PTE:AuNP over the number of extra AuNPs required for those multiple PTE-AuNPs. Error ranges removed for clarity but are in referenced publication. Initial values draw from Breger et al. and utilized for subsequent analysis here [76].

Table A3. Price comparison, using data from Sigma-Aldrich (St. Louis, MO, USA), accessed 22 November 2019, focusing on AuNP stabilized suspension in citrate buffer. All 100 mL samples were $321.

"A"	"B"	"C"	"D"	"E"	"F"	"G"	"H"
AuNP Dia. (nm)	**Approx. Concentration (AuNP/mL)**	**AuNPs in 100 mL**	**Price per AuNP ($)**	**Break-Even Price per Enzyme ($)**	**Break-Even Price per 1 mg 33 kDa Enzyme ($)**	**Cost Savings if $200/mg Enzyme, 1 µmol AuNP ($)**	**Code**
-	-	("**B**") * 100	$321/("**C**")	("**D**")/("**E**" in Table A2)	[[("**E**")*(6.022 × 10^{23})]/33,000]/1000	[6600*("**E**" in Table A2)]-[("**D**")*(6.022 × 10^{17})]	-
5	5.50×10^{13}	5.50×10^{15}	5.84×10^{-14}	5.06×10^{-15}	$92.27	41,035	741,949
10	6.00×10^{12}	6.00×10^{14}	5.35×10^{-13}	1.00×10^{-14}	$182.78	30,360	741,957
20	6.54×10^{11}	6.54×10^{13}	4.91×10^{-12}	3.30×10^{-14}	$602.41	Negative	741,965
50[1]	3.50×10^{10}	3.50×10^{12}	9.17×10^{-11}	8.96×10^{-14}	$1635.71	Negative	742,007
100	3.80×10^{9}	3.80×10^{11}	8.45×10^{-10}	4.02×10^{-13}	$7328.34	Negative	742,031

Based on data in Table 5 based on data from Breger et al. First row denotes columns for reference. Second row denotes column titles. Third row denotes calculations. Note that cost values are estimates only, and this table is presented as an illustrative exercise—cost values are likely to change with scale and source, and these data do not account for aspects such as desired process concentrations, enzyme stability, and recovery/reuse. "AuNP dia. (nm)" is the nominal diameter of the AuNP. "Approx. concentration (AuNP/mL)" is from Sigma-Aldrich; "AuNPs in 100 mL" is the number of AuNPs in 100 mL, the amount sold for $321, calculated by multiplying the concentration by 100. "Price per AuNP ($)" is the cost of each AuNP, calculated by $321 divided by the number of AuNPs in 100 mL. "Break-even price per enzyme" is price per AuNP divided by the extra equivalent PTE (from Table 5). "Break-even price per 1 mg 33 kDa enzyme" is the "Break-even price per enzyme" multiplied by Avogadro's number 6.022 × 1023 divided by (33,000 × 1000). If the cost of enzyme is above this amount, money is saved with AuNPs. "Cost savings if $200/mg enzyme, 1 µmol AuNP" is the calculated savings if enzyme costs $200/mg, based on the (Extra) enzyme activity achieved when immobilized, and is for illustrative purposes only. "Code" is the code for the item from Sigma Aldrich (actual code adds on "−100ML", excluded for space). [1] Note that price information for a 50 nm diameter AuNP has been used in place of a 55 nm diameter AuNP as this information was available from Sigma-Aldrich (https://www.sigmaaldrich.com/united-states.html; St. Louis, MO, USA). Initial values draw from Breger et al., and are utilized for subsequent analysis here [76].

References

1. Purich, D.L. *Enzyme Kinetics: Catalysis and Control: A Reference of Theory and Best-Practice Methods*; Elsevier Science: London, UK, 2010.
2. Bornscheuer, U.T.; Huisman, G.W.; Kazlauskas, R.J.; Lutz, S.; Moore, J.C.; Robins, K. Engineering the third wave of biocatalysis. *Nature* **2012**, *485*, 185–194. [CrossRef] [PubMed]
3. Chen, R.; Chen, Q.; Kim, H.; Siu, K.H.; Sun, Q.; Tsai, S.L.; Chen, W. Biomolecular scaffolds for enhanced signaling and catalytic efficiency. *Curr. Opin. Biotechnol.* **2014**, *28*, 59–68. [CrossRef] [PubMed]
4. Ellis, G.A.; Klein, W.P.; Lasarte-Aragonés, G.; Thakur, M.; Walper, S.A.; Medintz, I.L. Artificial multienzyme scaffolds: Pursuing *in vitro* substrate channeling with an overview of current progress. *ACS Catal.* **2019**, *9*, 10812–10869. [CrossRef]
5. Faber, K. *Biotransformations in Organic Chemistry*; Springer: Berlin/Heidelberg, Germany; New York, NY, USA, 2011.
6. Richter, M.; Schulenburg, C.; Jankowska, D.; Heck, T.; Faccio, G. Novel materials through Nature's catalysts. *Mater. Today* **2015**, *18*, 459–467. [CrossRef]
7. Schmid, A.; Dordick, J.S.; Hauer, B.; Kiener, A.; Wubbolts, M.; Witholt, B. Industrial biocatalysis today and tomorrow. *Nature* **2001**, *409*, 258–268. [CrossRef]
8. Walper, S.A.; Lasarte Aragonés, G.; Sapsford, K.E.; Brown, C.W., III; Rowland, C.E.; Breger, J.C.; Medintz, I.L. Detecting Biothreat Agents: From Current Diagnostics to Developing Sensor Technologies. *ACS Sens.* **2018**, *3*, 1894–2024. [CrossRef]
9. Alves, N.J.; Moore, M.; Johnson, B.J.; Dean, S.N.; Turner, K.B.; Medintz, I.L.; Walper, S.A. Environmental Decontamination of a Chemical Warfare Simulant Utilizing a Membrane Vesicle-Encapsulated Phosphotriesterase. *ACS Appl. Mater. Interfaces* **2018**, *10*, 15712–15719. [CrossRef]
10. Bulutoglu, B.; Garcia, K.E.; Wu, F.; Minteer, S.D.; Banta, S. Direct Evidence for Metabolon Formation and Substrate Channeling in Recombinant TCA Cycle Enzymes. *ACS Chem. Biol.* **2016**, *11*, 2847–2853. [CrossRef]
11. Rabe, K.S.; Muller, J.; Skoupi, M.; Niemeyer, C.M. Cascades in Compartments: En Route to Machine-Assisted Biotechnology. *Angew. Chem. Int. Ed. Engl.* **2017**, *56*, 13574–13589. [CrossRef]
12. Hwang, E.T.; Lee, S. Multienzymatic Cascade Reactions via Enzyme Complex by Immobilization. *ACS Catal.* **2019**, *9*, 4402–4425. [CrossRef]
13. Sperl, J.M.; Sieber, V. Multienzyme Cascade Reactions—Status and Recent Advances. *ACS Catal.* **2018**, *8*, 2385–2396. [CrossRef]
14. Zhang, Y.; Ge, J.; Liu, Z. Enhanced Activity of Immobilized or Chemically Modified Enzymes. *ACS Catal.* **2015**, *5*, 4503–4513. [CrossRef]
15. Höldrich, M.; Sievers-Engler, A.; Lämmerhofer, M. Gold nanoparticle-conjugated pepsin for efficient solution-like heterogeneous biocatalysis in analytical sample preparation protocols. *Anal. Bioanal. Chem.* **2016**, *408*, 5415–5427. [CrossRef] [PubMed]
16. Roco, M.C.; Williams, R.S.; Alivisatos, P. (Eds.) *Nanotechnology Research Directions: IWGN Worksop Report*; Vision for Nanotechnology R&D in the Next Decade; US National Science and Technology Council: Washington, DC, USA, 2000.
17. Alves, N.J.; Turner, K.B.; Medintz, I.L.; Walper, S.A. Protecting enzymatic function through directed packaging into bacterial outer membrane vesicles. *Sci. Rep.* **2016**, *6*, 24866. [CrossRef]
18. Schoffelen, S.; van Hest, J.C. Chemical approaches for the construction of multi-enzyme reaction systems. *Curr. Opin. Struct. Biol.* **2013**, *23*, 613–621. [CrossRef]
19. Vranish, J.N.; Ancona, M.G.; Oh, E.; Susumu, K.; Lasarte Aragonés, G.; Breger, J.C.; Walper, S.A.; Medintz, I.L. Enhancing Coupled Enzymatic Activity by Colocalization on Nanoparticle Surfaces: Kinetic Evidence for Directed Channeling of Intermediates. *ACS Nano* **2018**, *12*, 7911–7926. [CrossRef]
20. Zhang, Y.; Hess, H. Toward Rational Design of High-efficiency Enzyme Cascades. *ACS Catal.* **2017**, *7*, 6018–6027. [CrossRef]
21. Zhang, Y.; Tsitkov, S.; Hess, H. Proximity does not contribute to activity enhancement in the glucose oxidase-horseradish peroxidase cascade. *Nat Commun* **2016**, *7*, 13982. [CrossRef]
22. Vranish, J.N.; Ancona, M.G.; Walper, S.A.; Medintz, I.L. Pursuing the Promise of Enzymatic Enhancement with Nanoparticle Assemblies. *Langmuir* **2018**, *34*, 2901–2925. [CrossRef]
23. Berg, H.C. *Random Walks in Biology*; Princeton University Press: Princeton, NJ, USA, 1983.

24. Idan, O.; Hess, H. Origins of Activity Enhancement in Enzyme Cascades on Scaffolds. *ACS Nano* **2013**, *7*, 8658–8665. [CrossRef]
25. Idan, O.; Hess, H. Engineering enzymatic cascades on nanoscale scaffolds. *Curr. Opin. Biotechnol.* **2013**, *24*, 606–611. [CrossRef] [PubMed]
26. Ovádi, J. Physiological significance of metabolic channeling. *J. Theor. Biol.* **1991**, *152*, 1–22. [CrossRef]
27. Spivey, H.O.; Ovádi, J. Substrate Channeling. *Methods* **1999**, *19*, 306–321. [CrossRef] [PubMed]
28. Wheeldon, I.; Minteer, S.D.; Banta, S.; Barton, S.C.; Atanassov, P.; Sigman, M. Substrate channelling as an approach to cascade reactions. *Nat. Chem.* **2016**, *8*, 299–309. [CrossRef]
29. Lata, J.P.; Gao, L.; Mukai, C.; Cohen, R.; Nelson, J.L.; Anguish, L.; Coonrod, S.; Travis, A.J. Effects of Nanoparticle Size on Multilayer Formation and Kinetics of Tethered Enzymes. *Bioconjug. Chem.* **2015**, *26*, 1931–1938. [CrossRef]
30. Vertegel, A.A.; Siegel, R.W.; Dordick, J.S. Silica Nanoparticle Size Influences the Structure and Enzymatic Activity of Adsorbed Lysozyme. *Langmuir* **2004**, *20*, 6800–6807. [CrossRef]
31. Tadepalli, S.; Wang, Z.; Slocik, J.; Naik, R.R.; Singamaneni, S. Effect of size and curvature on the enzyme activity of bionanoconjugates. *Nanoscale* **2017**, *9*, 15666–15672. [CrossRef]
32. Algar, W.R.; Prasuhn, D.E.; Stewart, M.H.; Jennings, T.L.; Blanco-Canosa, J.B.; Dawson, P.E.; Medintz, I.L. The controlled display of biomolecules on nanoparticles: A challenge suited to bioorthogonal chemistry. *Bioconjug. Chem.* **2011**, *22*, 825–858. [CrossRef]
33. Boeneman, K.; Deschamps, J.R.; Buckhout-White, S.; Prasuhn, D.E.; Blanco-Canosa, J.B.; Dawson, P.E.; Stewart, M.H.; Susumu, K.; Goldman, E.R.; Ancona, M.; et al. Quantum Dot DNA Bioconjugates: Attachment Chemistry Strongly Influences the Resulting Composite Architecture. *ACS Nano* **2010**, *4*, 7253–7266. [CrossRef]
34. Hermanson, G.T. *Bioconjugate Techniques*, 3rd ed.; Academic Press: San Diego, CA, USA, 2013.
35. Medintz, I. Universal tools for biomolecular attachment to surfaces. *Nat. Mater.* **2006**, *5*, 842. [CrossRef]
36. Roberts, C.C.; Chang, C.E. Modeling of enhanced catalysis in multienzyme nanostructures: Effect of molecular scaffolds, spatial organization, and concentration. *J. Chem. Theory Comput.* **2015**, *11*, 286–292. [CrossRef] [PubMed]
37. Walper, S.A.; Turner, K.B.; Medintz, I.L. Enzymatic bioconjugation of nanoparticles: Developing specificity and control. *Curr. Opin. Biotechnol.* **2015**, *34*, 232–241. [CrossRef] [PubMed]
38. Ansari, S.A.; Husain, Q. Potential applications of enzymes immobilized on/in nano materials: A review. *Biotechnol. Adv.* **2012**, *30*, 512–523. [CrossRef] [PubMed]
39. Breger, J.C.; Ancona, M.G.; Walper, S.A.; Oh, E.; Susumu, K.; Stewart, M.H.; Deschamps, J.R.; Medintz, I.L. Understanding How Nanoparticle Attachment Enhances Phosphotriesterase Kinetic Efficiency. *ACS Nano* **2015**, *9*, 8491–8503. [CrossRef] [PubMed]
40. Brown, C.W., III; Oh, E.; Hastman, D.A., Jr.; Walper, S.A.; Susumu, K.; Stewart, M.H.; Deschamps, J.R.; Medintz, I.L. Kinetic enhancement of the diffusion-limited enzyme beta-galactosidase when displayed with quantum dots. *RSC Adv.* **2015**, *5*, 93089–93094. [CrossRef]
41. Claussen, J.C.; Malanoski, A.; Breger, J.C.; Oh, E.; Walper, S.A.; Susumu, K.; Goswami, R.; Deschamps, J.R.; Medintz, I.L. Probing the Enzymatic Activity of Alkaline Phosphatase within Quantum Dot Bioconjugates. *J. Phys. Chem. C* **2015**, *119*, 2208–2221. [CrossRef]
42. Ding, S.W.; Cargill, A.A.; Medintz, I.L.; Claussen, J.C. Increasing the activity of immobilized enzymes with nanoparticle conjugation. *Curr. Opin. Biotechnol.* **2015**, *34*, 242–250. [CrossRef]
43. Johnson, B.J.; Algar, W.R.; Malanoski, A.P.; Ancona, M.G.; Medintz, I.L. Understanding enzymatic acceleration at nanoparticle interfaces: Approaches and challenges. *Nano Today* **2014**, *9*, 102–131. [CrossRef]
44. Vranish, J.N.; Ancona, M.G.; Oh, E.; Susumu, K.; Medintz, I.L. Enhancing coupled enzymatic activity by conjugating one enzyme to a nanoparticle. *Nanoscale* **2017**, *9*, 5172–5187. [CrossRef]
45. Lin, J.-L.; Wheeldon, I. Kinetic Enhancements in DNA–Enzyme Nanostructures Mimic the Sabatier Principle. *ACS Catal.* **2013**, *3*, 560–564. [CrossRef]
46. Wilner, O.I.; Weizmann, Y.; Gill, R.; Lioubashevski, O.; Freeman, R.; Willner, I. Enzyme cascades activated on topologically programmed DNA scaffolds. *Nat. Nanotechnol.* **2009**, *4*, 249–254. [CrossRef] [PubMed]
47. Klein, W.P.; Thomsen, R.P.; Turner, K.B.; Walper, S.A.; Vranish, J.; Kjems, J.; Ancona, M.G.; Medintz, I.L. Enhanced Catalysis from Multienzyme Cascades Assembled on a DNA Origami Triangle. *ACS Nano* **2019**. [CrossRef] [PubMed]

48. Zhao, Z.; Fu, J.; Dhakal, S.; Johnson-Buck, A.; Liu, M.; Zhang, T.; Woodbury, N.W.; Liu, Y.; Walter, N.G.; Yan, H. Nanocaged enzymes with enhanced catalytic activity and increased stability against protease digestion. *Nat. Commun.* **2016**, *7*, 10619–10627. [CrossRef] [PubMed]
49. Dudley, Q.M.; Karim, A.S.; Jewett, M.C. Cell-free metabolic engineering: Biomanufacturing beyond the cell. *Biotechnol. J.* **2015**, *10*, 69–82. [CrossRef] [PubMed]
50. Myung, S.; You, C.; Zhang, Y.H.P. Recyclable cellulose-containing magnetic nanoparticles: Immobilization of cellulose-binding module-tagged proteins and a synthetic metabolon featuring substrate channeling. *J. Mater. Chem. B* **2013**, *1*, 4419–4427. [CrossRef]
51. Mohammadi, M.; Rezaei Mokarram, R.; Ghorbani, M.; Hamishehkar, H. Inulinase immobilized gold-magnetic nanoparticles as a magnetically recyclable biocatalyst for facial and efficient inulin biotransformation to high fructose syrup. *Int. J. Biol. Macromol.* **2019**, *123*, 846–855. [CrossRef]
52. Sahoo, B.; Sahu, S.K.; Bhattacharya, D.; Dhara, D.; Pramanik, P. A novel approach for efficient immobilization and stabilization of papain on magnetic gold nanocomposites. *Colloids Surf. B Biointerfaces* **2013**, *101*, 280–289. [CrossRef]
53. Sweetlove, L.J.; Fernie, A.R. The spatial organization of metabolism within the plant cell. *Annu. Rev. Plant Biol.* **2013**, *64*, 723–746. [CrossRef]
54. Sweetlove, L.J.; Fernie, A.R. The role of dynamic enzyme assemblies and substrate channelling in metabolic regulation. *Nat. Commun.* **2018**, *9*, 2136–2147. [CrossRef]
55. Dueber, J.E.; Wu, G.C.; Malmirchegini, G.R.; Moon, T.S.; Petzold, C.J.; Ullal, A.V.; Prather, K.L.; Keasling, J.D. Synthetic protein scaffolds provide modular control over metabolic flux. *Nat. Biotechnol.* **2009**, *27*, 753–759. [CrossRef]
56. Haimovitz, R.; Barak, Y.; Morag, E.; Voronov-Goldman, M.; Shoham, Y.; Lamed, R.; Bayer, E.A. Cohesin-dockerin microarray: Diverse specificities between two complementary families of interacting protein modules. *Proteomics* **2008**, *8*, 968–979. [CrossRef] [PubMed]
57. Pagès, S.; Bélaïch, A.; Bélaïch, J.-P.; Morag, E.; Lamed, R.; Shoham, Y.; Bayer, E.A. Species-Specificity of the Cohesin-Dockerin Interaction Between *Clostridium thermocellum* and *Clostridium cellulolyticum*: Prediction of Specificity Determinants of the Dockerin Domain. *Proteins Struct. Funct. Bioinform.* **1997**, *29*, 517–527. [CrossRef]
58. Tsai, S.L.; Oh, J.; Singh, S.; Chen, R.; Chen, W. Functional assembly of minicellulosomes on the *Saccharomyces cerevisiae* cell surface for cellulose hydrolysis and ethanol production. *Appl. Environ. Microbiol.* **2009**, *75*, 6087–6093. [CrossRef] [PubMed]
59. Campbell, A.S.; Dong, C.; Meng, F.; Hardinger, J.; Perhinschi, G.; Wu, N.; Dinu, C.Z. Enzyme catalytic efficiency: A function of bio-nano interface reactions. *ACS Appl Mater Interfaces* **2014**, *6*, 5393–5403. [CrossRef]
60. Hinterwirth, H.; Lindner, W.; Lämmerhofer, M. Bioconjugation of trypsin onto gold nanoparticles: Effect of surface chemistry on bioactivity. *Anal. Chim. Acta* **2012**, *733*, 90–97. [CrossRef]
61. Hondred, J.A.; Breger, J.C.; Garland, N.T.; Oh, E.; Susumu, K.; Walper, S.A.; Medintz, I.L.; Claussen, J.C. Enhanced Enzyme Activity of Phosphotriesterase Trimer Conjugated on Gold Nanoparticles for Pesticide Detection. *Analyst* **2017**, *142*, 3261–3271. [CrossRef]
62. Pfeiffer, C.; Rehbock, C.; Huhn, D.; Carrillo-Carrion, C.; de Aberasturi, D.J.; Merk, V.; Barcikowski, S.; Parak, W.J. Interaction of colloidal nanoparticles with their local environment: The (ionic) nanoenvironment around nanoparticles is different from bulk and determines the physico-chemical properties of the nanoparticles. *J. R. Soc. Interface* **2014**, *11*, 20130931. [CrossRef]
63. Shikha, S.; Thakur, K.G.; Bhattacharyya, M.S. Facile fabrication of lipase to amine functionalized gold nanoparticles to enhance stability and activity. *RSC Adv.* **2017**, *7*, 42845–42855. [CrossRef]
64. Zobel, M.; Neder, R.B.; Kimber, S.A.J. Universal solvent restructuring induced by colloidal nanoparticles. *Science* **2015**, *347*, 292–294. [CrossRef]
65. Algar, W.R.; Dawson, P.E.; Medintz, I.L. *Chemoselective and Bioorthogonal Ligation Reactions: Concepts and Applications*; Wiley VCH: Weinheim, Germany, 2017.
66. Kozlowski, R.; Ragupathi, A.; Dyer, R.B. Characterizing the Surface Coverage of Protein-Gold Nanoparticle Bioconjugates. *Bioconjug. Chem.* **2018**, *29*, 2691–2700. [CrossRef]
67. Medintz, I.L.; Goldman, E.R.; Lassman, M.E.; Hayhurst, A.; Kusterbeck, A.W.; Deschamps, J.R. Self-assembled TNT biosensor based on modular multifunctional surface-tethered components. *Anal. Chem.* **2005**, *77*, 365–372. [CrossRef] [PubMed]

68. Brown, C.W., III; Samanta, A.; Díaz, S.A.; Buckhout-White, S.; Walper, S.A.; Goldman, E.R.; Medintz, I.L. Dendrimeric DNA Nanostructures as Scaffolds for Efficient Bidirectional BRET–FRET Cascades. *Adv. Opt. Mater.* **2017**, *5*, 1700181–1700193. [CrossRef]
69. Sapsford, K.E.; Pons, T.; Medintz, I.L.; Higashiya, S.; Brunel, F.M.; Dawson, P.E.; Mattoussi, H. Kinetics of Metal-Affinity Driven Self-Assembly between Proteins or Peptides and CdSe−ZnS Quantum Dots. *J. Phys. Chem. C* **2007**, *111*, 11528–11538. [CrossRef]
70. Nieba, L.; Nieba-Axmann, S.E.; Persson, A.; Hämäläinen, M.; Edebratt, F.; Hansson, A.; Lidholm, J.; Magnusson, K.; Karlsson, Å.F.; Plückthun, A. BIACORE Analysis of Histidine-Tagged Proteins Using a Chelating NTA Sensor Chip. *Anal. Biochem.* **1997**, *252*, 217–228. [CrossRef]
71. Fu, J.; Yang, Y.R.; Johnson-Buck, A.; Liu, M.; Liu, Y.; Walter, N.G.; Woodbury, N.W.; Yan, H. Multi-enzyme complexes on DNA scaffolds capable of substrate channelling with an artificial swinging arm. *Nat. Nanotechnol.* **2014**, *9*, 531. [CrossRef]
72. Goldstein, D.E.; Little, R.R.; Lorenz, R.A.; Malone, J.I.; Nathan, D.; Peterson, C.M.; Sacks, D.B. Tests of Glycemia in Diabetes. *Diabetes Care* **2004**, *27*, 1761–1773. [CrossRef]
73. Müller, J.; Niemeyer, C.M. DNA-directed assembly of artificial multienzyme complexes. *Biochem. Biophys. Res. Commun.* **2008**, *377*, 62–67. [CrossRef]
74. Nguyen, L.T.; Yang, K.L. Combined cross-linked enzyme aggregates of horseradish peroxidase and glucose oxidase for catalyzing cascade chemical reactions. *Enzym. Microb. Technol.* **2017**, *100*, 52–59. [CrossRef]
75. Liu, Y.; Hickey, D.P.; Guo, J.-Y.; Earl, E.; Abdellaoui, S.; Milton, R.D.; Sigman, M.S.; Minteer, S.D.; Calabrese Barton, S. Substrate Channeling in an Artificial Metabolon: A Molecular Dynamics Blueprint for an Experimental Peptide Bridge. *ACS Catal.* **2017**, *7*, 2486–2493. [CrossRef]
76. Breger, J.C.; Oh, E.; Susumu, K.; Klein, W.P.; Walper, S.A.; Ancona, M.G.; Medintz, I.L. Nanoparticle Size Influences Localized Enzymatic Enhancement-A Case Study with Phosphotriesterase. *Bioconjug. Chem.* **2019**, *30*, 2060–2074. [CrossRef]
77. Jia, H.; Zhu, G.; Wang, P. Catalytic behaviors of enzymes attached to nanoparticles: The effect of particle mobility. *Biotechnol. Bioeng.* **2003**, *84*, 406–414. [CrossRef] [PubMed]
78. Wu, C.S.; Lee, C.C.; Wu, C.T.; Yang, Y.S.; Ko, F.H. Size-modulated catalytic activity of enzyme-nanoparticle conjugates: A combined kinetic and theoretical study. *Chem. Commun.* **2011**, *47*, 7446–7448. [CrossRef] [PubMed]
79. Park, H.J.; McConnell, J.T.; Boddohi, S.; Kipper, M.J.; Johnson, P.A. Synthesis and characterization of enzyme-magnetic nanoparticle complexes: Effect of size on activity and recovery. *Colloids Surf. B Biointerfaces* **2011**, *83*, 198–203. [CrossRef] [PubMed]
80. Zhang, J.; Zhang, F.; Yang, H.; Huang, X.; Liu, H.; Zhang, J.; Guo, S. Graphene oxide as a matrix for enzyme immobilization. *Langmuir* **2010**, *26*, 6083–6085. [CrossRef]
81. Breger, J.C.; Buckhout-White, S.; Walper, S.A.; Oh, E.; Susumu, K.; Ancona, M.G.; Medintz, I.L. Assembling high activity phosphotriesterase composites using hybrid nanoparticle peptide-DNA scaffolded architectures. *Nano Futures* **2017**, *1*, 011002. [CrossRef]
82. Breger, J.C.; Walper, S.A.; Oh, E.; Susumu, K.; Stewart, M.H.; Deschamps, J.R.; Medintz, I.L. Quantum Dot Display Enhances Activity of a Phosphotriesterase Trimer. *Chem. Commun.* **2015**, *51*, 6403–6406. [CrossRef]
83. Cornish-Bowden, A. *Fundamentals of Enzyme Kinetics*, 4th ed.; Wiley-Blackwell: Weinheim, Germany, 2012.
84. Mukai, C.; Gao, L.; Nelson, J.L.; Lata, J.P.; Cohen, R.; Wu, L.; Hinchman, M.M.; Bergkvist, M.; Sherwood, R.W.; Zhang, S.; et al. Biomimicry Promotes the Efficiency of a 10-Step Sequential Enzymatic Reaction on Nanoparticles, Converting Glucose to Lactate. *Angew. Chem. Int. Ed. Engl.* **2017**, *56*, 235–238. [CrossRef]
85. Castellana, M.; Wilson, M.Z.; Xu, Y.; Joshi, P.; Cristea, I.M.; Rabinowitz, J.D.; Gitai, Z.; Wingreen, N.S. Enzyme clustering accelerates processing of intermediates through metabolic channeling. *Nat. Biotechnol.* **2014**, *32*, 1011–1018. [CrossRef]
86. Medintz, I.L.; Uyeda, H.T.; Goldman, E.R.; Mattoussi, H. Quantum dot bioconjugates for imaging, labelling, and sensing. *Nat. Mater.* **2005**, *4*, 435–446. [CrossRef]
87. Petryayeva, E.; Algar, W.R.; Medintz, I.L. Quantum dots in bioanalysis: A review of applications across various platforms for fluorescence spectroscopy and imaging. *Appl. Spectrosc.* **2013**, *67*, 215–252. [CrossRef]

88. Hildebrandt, N.; Spillmann, C.M.; Algar, W.R.; Pons, T.; Stewart, M.H.; Oh, E.; Susumu, K.; Díaz, S.A.; Delehanty, J.B.; Medintz, I.L. Energy Transfer with Semiconductor Quantum Dot Bioconjugates: A Versatile Platform for Biosensing, Energy Harvesting, and Other Developing Applications. *Chem. Rev.* **2017**, *117*, 536–711. [CrossRef] [PubMed]
89. Malanoski, A.P.; Breger, J.C.; Brown, C.W.I.; Deschamps, J.R.; Susumu, K.; Oh, E.; Anderson, G.P.; Walper, S.A.; Medintz, I.L. Kinetic enhancement in high-activity enzyme complexes attached to nanoparticles. *Nanoscale Horiz.* **2017**, *2*, 241–252. [CrossRef]
90. Díaz, S.A.; Sen, S.; Boeneman Gemmill, K.; Brown, C.W., III; Oh, E.; Susumu, K.; Stewart, M.H.; Breger, J.C.; Lasarte Aragones, G.; Field, L.D.; et al. Elucidating Surface Ligand-Dependent Kinetic Enhancement of Proteolytic Activity at Surface-Modified Quantum Dots. *ACS Nano* **2017**, *11*, 5884–5896. [CrossRef] [PubMed]
91. Blanco-Canosa, J.B.; Wu, M.; Susumu, K.; Petryayeva, E.; Jennings, T.L.; Dawson, P.E.; Algar, W.R.; Medintz, I.L. Recent progress in the bioconjugation of quantum dots. *Coord. Chem. Rev.* **2014**, *263–264*, 101–137. [CrossRef]
92. Gemmill, K.B.; Deschamps, J.R.; Delehanty, J.B.; Susumu, K.; Stewart, M.H.; Glaven, R.H.; Anderson, G.P.; Goldman, E.R.; Huston, A.L.; Medintz, I.L. Optimizing Protein Coordination to Quantum Dots with Designer Peptidyl Linkers. *Bioconjug. Chem.* **2013**, *24*, 269–281. [CrossRef] [PubMed]
93. Susumu, K.; Oh, E.; Delehanty, J.B.; Blanco-Canosa, J.B.; Johnson, B.J.; Jain, V.; Hervey, W.J.T.; Algar, W.R.; Boeneman, K.; Dawson, P.E.; et al. Multifunctional compact zwitterionic ligands for preparing robust biocompatible semiconductor quantum dots and gold nanoparticles. *J. Am. Chem. Soc.* **2011**, *133*, 9480–9496. [CrossRef] [PubMed]
94. Susumu, K.; Oh, E.; Delehanty, J.B.; Pinaud, F.; Gemmill, K.B.; Walper, S.; Breger, J.; Schroeder, M.J.; Stewart, M.H.; Jain, V.; et al. A New Family of Pyridine-Appended Multidentate Polymers as Hydrophilic Surface Ligands for Preparing Stable Biocompatible Quantum Dots. *Chem. Mater.* **2014**, *26*, 5327–5344. [CrossRef]
95. Das, K.; Rawat, K.; Patel, R.; Bohidar, H.B. Size-dependent CdSe quantum dot–lysozyme interaction and effect on enzymatic activity. *RSC Adv.* **2016**, *6*, 46744–46754. [CrossRef]
96. Kang, W.; Liu, J.; Wang, J.; Nie, Y.; Guo, Z.; Xia, J. Cascade biocatalysis by multienzyme-nanoparticle assemblies. *Bioconjug. Chem* **2014**, *25*, 1387–1394. [CrossRef]
97. Tsai, S.L.; Park, M.; Chen, W. Size-modulated synergy of cellulase clustering for enhanced cellulose hydrolysis. *Biotechnol. J.* **2013**, *8*, 257–261. [CrossRef]
98. Algar, W.R.; Ancona, M.; Malanoski, A.P.; Susumu, K.; Medintz, I.L. Assembly of a Concentric Förster Resonance Energy Transfer Relay on a Quantum Dot Scaffold: Characterization and Application to Multiplexed Protease Sensing. *ACS Nano* **2012**, *6*, 11044–11058. [CrossRef] [PubMed]
99. Algar, W.R.; Jeen, T.; Massey, M.; Peveler, W.J.; Asselin, J. Small Surface, Big Effects, and Big Challenges: Toward Understanding Enzymatic Activity at the Inorganic Nanoparticle-Substrate Interface. *Langmuir* **2019**, *35*, 7067–7091. [CrossRef] [PubMed]
100. Algar, W.R.; Krull, U.J. Quantum dots as donors in fluorescence resonance energy transfer for the bioanalysis of nucleic acids, proteins, and other biological molecules. *Anal. Bioanal. Chem.* **2008**, *391*, 1609–1618. [CrossRef] [PubMed]
101. Algar, W.R.; Krull, U.J. New opportunities in multiplexed optical bioanalyses using quantum dots and donor-acceptor interactions. *Anal. Bioanal. Chem.* **2010**, *398*, 2439–2449. [CrossRef]
102. Algar, W.R.; Malanoski, A.P.; Susumu, K.; Stewart, M.H.; Hildebrandt, N.; Medintz, I.L. Multiplexed tracking of protease activity using a single color of quantum dot vector and a time-gated Forster resonance energy transfer relay. *Anal. Chem.* **2012**, *84*, 10136–10146. [CrossRef]
103. Algar, W.R.; Malonoski, A.; Deschamps, J.R.; Blanco-Canosa, J.B.; Susumu, K.; Stewart, M.H.; Johnson, B.J.; Dawson, P.E.; Medintz, I.L. Proteolytic activity at quantum dot-conjugates: Kinetic analysis reveals enhanced enzyme activity and localized interfacial "hopping". *Nano Lett.* **2012**, *12*, 3793–3802. [CrossRef]
104. Algar, W.R.; Susumu, K.; Delehanty, J.B.; Medintz, I.L. Semiconductor quantum dots in bioanalysis: Crossing the valley of death. *Anal. Chem.* **2011**, *83*, 8826–8837. [CrossRef]
105. Algar, W.R.; Tavares, A.J.; Krull, U.J. Beyond labels: A review of the application of quantum dots as integrated components of assays, bioprobes, and biosensors utilizing optical transduction. *Anal. Chim. Acta* **2010**, *673*, 1–25. [CrossRef]

106. Algar, W.R.; Wegner, D.; Huston, A.L.; Blanco-Canosa, J.B.; Stewart, M.H.; Armstrong, A.; Dawson, P.E.; Hildebrandt, N.; Medintz, I.L. Quantum dots as simultaneous acceptors and donors in time-gated Forster resonance energy transfer relays: Characterization and biosensing. *J. Am. Chem. Soc.* **2012**, *134*, 1876–1891. [CrossRef]
107. Jeen, T.; Algar, W.R. Mimicking Cell Surface Enhancement of Protease Activity on the Surface of a Quantum Dot Nanoparticle. *Bioconjug. Chem.* **2018**, *29*, 3783–3792. [CrossRef]
108. Petryayeva, E.; Jeen, T.; Algar, W.R. Optimization and Changes in the Mode of Proteolytic Turnover of Quantum Dot-Peptide Substrate Conjugates through Moderation of Interfacial Adsorption. *ACS Appl. Mater. Interfaces* **2017**, *9*, 30359–30372. [CrossRef] [PubMed]
109. Sapsford, K.E.; Algar, W.R.; Berti, L.; Gemmill, K.B.; Casey, B.J.; Oh, E.; Stewart, M.H.; Medintz, I.L. Functionalizing Nanoparticles with Biological Molecules: Developing Chemistries that Facilitate Nanotechnology. *Chem. Rev.* **2013**, *113*, 1904–2074. [CrossRef] [PubMed]
110. Wu, M.; Algar, W.R. Acceleration of proteolytic activity associated with selection of thiol ligand coatings on quantum dots. *ACS Appl. Mater. Interfaces* **2015**, *7*, 2535–2545. [CrossRef] [PubMed]
111. Höldrich, M.; Liu, S.; Epe, M.; Lämmerhofer, M. Taylor dispersion analysis, resonant mass measurement and bioactivity of pepsin-coated gold nanoparticles. *Talanta* **2017**, *167*, 67–74. [CrossRef]
112. Liu, S.; Höldrich, M.; Sievers-Engler, A.; Horak, J.; Lämmerhofer, M. Papain-functionalized gold nanoparticles as heterogeneous biocatalyst for bioanalysis and biopharmaceuticals analysis. *Anal. Chim. Acta* **2017**, *963*, 33–43. [CrossRef]
113. Homaei, A.; Barkheh, H.; Sariri, R.; Stevanato, R. Immobilized papain on gold nanorods as heterogeneous biocatalysts. *Amino Acids* **2014**, *46*, 1649–1657. [CrossRef]
114. Liu, F.; Wang, L.; Wang, H.; Yuan, L.; Li, J.; Brash, J.L.; Chen, H. Modulating the activity of protein conjugated to gold nanoparticles by site-directed orientation and surface density of bound protein. *ACS Appl. Mater. Interfaces* **2015**, *7*, 3717–3724. [CrossRef]
115. Liu, F.; Cui, Y.; Wang, L.; Wang, H.; Yuan, Y.; Pan, J.; Chen, H.; Yuan, L. Temperature-Responsive Poly(N-isopropylacrylamide) Modified Gold Nanoparticle-Protein Conjugates for Bioactivity Modulation. *ACS Appl. Mater. Interfaces* **2015**, *7*, 11547–11554. [CrossRef]
116. Liu, F.; Xue, L.; Yuan, Y.; Pan, J.; Zhang, C.; Wang, H.; Brash, J.L.; Yuan, L.; Chen, H. Multifunctional nanoparticle-protein conjugates with controllable bioactivity and pH responsiveness. *Nanoscale* **2016**, *8*, 4387–4394. [CrossRef]
117. Ball, P.; Thompson, E.; Anderson, S.; Gwenin, V.; Gwenin, C. Time dependent HPLC analysis of the product ratio of enzymatically reduced prodrug CB1954 by a modified and immobilised nitroreductase. *Eur. J. Pharm. Sci.* **2019**, *127*, 217–224. [CrossRef]
118. Liu, S.; Horak, J.; Höldrich, M.; Lämmerhofer, M. Accurate and reliable quantification of the protein surface coverage on protein-functionalized nanoparticles. *Anal. Chim. Acta* **2017**, *989*, 29–37. [CrossRef] [PubMed]
119. Liu, S.; Lämmerhofer, M. Functionalized gold nanoparticles for sample preparation: A review. *Electrophoresis* **2019**, *40*, 2438–2461. [CrossRef] [PubMed]
120. Lassman, M.E.; Rahbar, A.; Medintz, I.L.; Ligler, F.S. Incorporation of18Oxygen into Peptide Mixtures and Analysis with Multi-Dimensional Chromatography and Mass-Spectroscopy. *Anal. Lett.* **2007**, *40*, 1864–1878. [CrossRef]
121. Li, Z.; Liu, F.; Yuan, Y.; Wu, J.; Wang, H.; Yuan, L.; Chen, H. Multifunctional gold nanoparticle layers for controllable capture and release of proteins. *Nanoscale* **2017**, *9*, 15407–15415. [CrossRef]